https://doi.org/10.5194/egusphere-2024-3480
Preprint. Discussion started: 6 December 2024

Glacier surge monitoring from temporally dense elevation time series: application to an ASTER dataset over the Karakoram region

Luc Beraud[1], Fanny Brun[1], Amaury Dehecq[1], Romain Hugonnet[2], and Prashant Shekhar[3]

[1]Université Grenoble Alpes, CNRS, IRD, Grenoble INP, INRAE, Institut des Géosciences de l'Environnement (IGE), 38000 Grenoble, France
[2]University of Washington, Civil and Environmental Engineering, Seattle, WA, USA
[3]Embry-Riddle Aeronautical University, Daytona Beach Campus, FL, USA

Correspondence: Luc Beraud (luc.beraud@univ-grenoble-alpes.fr, luc.beraud@protonmail.com)

Abstract.

Glacier surges are spectacular events that lead to surface elevation changes of tens of meter in a period of a few months to a few years, with different patterns of mass transport. Existing methods of elevation change estimate of surges, and subsequent quantification of their mass transported, rely on differencing pairs of digital elevation models (DEMs) that may not be acquired regularly in time. In this study, we propose a workflow to filter and interpolate a dense time series of DEMs specifically for the study of surge events. We test this workflow on a global 20-year dataset of DEMs from the optical satellite sensor Advanced Spaceborne Thermal Emission and Reflection Radiometer (ASTER). The multi-step procedure includes linear non-parametric Locally Weighted Regression and Smoothing Scatterplots (LOWESS) filtering and Approximation by Localized Penalized Splines (ALPS) interpolation. We run the workflow over the Karakoram mountain range (High Mountain Asia). We compare the produced dataset to previous studies for four selected surge events (surges of Hispar, Khurdopin, Kyagar and Yazghil glaciers). We demonstrate that our workflow captures thickness changes at monthly scale with detailed patterns of mass transportation. Such patterns includes surge front propagation, changes in dynamic balance line, and slow surge onset among others, and allows an unprecedentedly detailed description of glacier surges at the scale of a large region. The workflow preserves most of the elevation change signal, with underestimation or smoothing in a limited number of surge cases.

1 Introduction

Surge events are extreme cases of the continuous spectrum of glacier flow instabilities (Herreid and Truffer, 2016). Surges are quasi-periodic events characterised by an abnormally rapid glacier flow, lasting from several months to years (Cuffey and Paterson, 2010; Bhambri et al., 2017). They occur on a limited number of glaciers known as surge-type glaciers, which are clustered in a few regions of the globe, among which the Karakoram in High Mountain Asia in one of the cluster with the most of them (Sevestre and Benn, 2015; Guillet et al., 2022). Surges can occur on both land-terminating and tidewater glaciers and can be either polythermal or temperate (Cuffey and Paterson, 2010). The mechanisms behind the surge phenomenon (origin, surge trigger, etc.) are not yet fully understood and this subject continues to be the object of developments and theories (Benn et al., 2023; Terleth et al., 2021; Thøgersen et al., 2024; Crompton et al., 2018).

https://doi.org/10.5194/egusphere-2024-3480
Preprint. Discussion started: 6 December 2024

Surge events are often studied a posteriori with remote sensing data. Satellite imagery is used for visual mapping, to derive surface velocity maps or elevation change (Paul et al., 2022). Remote sensing data have been used in numerous studies, ranging from the inventorying of surge-type glaciers to detailed case studies (e.g., Guo et al., 2020; Round et al., 2017; Guillet et al., 2022; Bhambri et al., 2022). A large number of studies have used surface velocities derived from optical and radar satellites to estimate precise surge dates and evolution patterns (e.g., velocities over 2-3 weeks in Round et al. (2017), Guo et al. (2020)). Surface velocities are also used in combination with other data, such as elevation change data, to map surge-type glacier inventories (Guillet et al., 2022; Guo et al., 2022). The study of elevation changes can give some insight into the current state of a glacier in its surge cycle. A few surge-type glaciers may begin surging after a critical mass has built up in the reservoir (Kotlyakov et al., 2018; Lovell et al., 2018). Elevation data, and by extension surface slope, can be used to compute basal shear stress, which may play a critical role in the triggering of surges (Beaud et al., 2022; Thøgersen et al., 2024).

Temporally dense elevation time series from satellites covering a long period of time have recently become available for studying glacier elevation change. Such acquisitions started on about 2000, with now some time series spanning on more than two decades, long enough to capture entirely a number of surge events. Elevation measurements from altimetry mission (laser or radar, such as ICESat-2, CryoSat-2 etc.) benefits from good temporal resolutions, but their spatial resolution and coverage does not perhaps permit the spatial study of surges as effectively as higher resolution DEMs (e.g., Wang et al., 2021; Yue et al., 2023; Lai and Wang, 2022). The use of suitable digital elevation models (DEMs) for the study of surges is often limited to a few dates or specific case studies. Several studies use temporally dense SAR time series on case studies, usually without time series filtering technique (Round et al., 2017; Wendt et al., 2017; Zhang et al., 2023). Dense elevation time series have been used in studies of long-term elevation trends and multi-year glacier mass balance (e.g., Brun et al., 2017; Shean et al., 2020; Hugonnet et al., 2021). However, surges are short-term events with important elevation changes, and surge-type elevation time series are non-linear. The retrieval of mass transfer variations happening during single surge events requires dense elevation time series with a resolution of one or a few months in principle. However, optical stereo satellite sensors with systematic acquisitions worldwide and with a high temporal resolution, typically Advanced Spaceborne Thermal Emission and Reflection Radiometer (ASTER) imagery, have rather coarse resolutions (> 10 m). The DEMs derived from these sensors have elevation precisions of similar magnitude and sometimes large artefacts (e.g., cloud sensitivity, jitter, difficulty of photogrammetric correlation...). They need techniques of filtering that preserve surge signals (i.e., preserve elevation observations before, during and after the surge). Basic thresholds and linear methods might misinterpret surge observations as outliers. Also, the volume transported or slope should be computed at consistent dates across a whole glacier. Thus, a final step of interpolation is required.

Various approaches have been implemented in the context of glacier elevation time series analysis. Hugonnet et al. (2021) have implemented a complex workflow for ASTER elevation time series over glaciers at global scale. It captures limited non-linear elevation change, but fails to accurately reflect sudden changes associated with surge events. In Hugonnet et al. (2021) filtering and interpolation methods involve Gaussian Process Regression, based on a complex kernel defined by the variance of non-surge-type elevation changes. It results in a dataset where the elevation change of surge-type glaciers is underestimated. Shekhar et al. (2021) developed a spline-based approximation framework to model elevation changes with heterogeneous data, that can also be used for filtering. Another approach from Wang and Kääb (2015) detects outliers, when no reference elevation

https://doi.org/10.5194/egusphere-2024-3480
Preprint. Discussion started: 6 December 2024

exists, with a RANSAC (RANdom SAmple Consensus) algorithm. Other methods exist for the processing of time series of glacier surface velocity. Charrier et al. (2022) invert velocities using temporal closure of the displacement. It takes advantage of overlapping and multiple velocity measurements by combining these observations though an iterative reweighted least square to recompose a regular, optimized time series. Local regressions can be used with equivalent applicability for elevation, such as linear non-parametric local regression (LOWESS) that has been used for glacier surface velocities (Derkacheva et al., 2020). Existing procedures have different abilities and specific requirements to work properly with available DEM datasets from stereo imagery for the study of surges. To accurately estimate the parameters of surge events, existing methods must be adapted into a workflow that can process regional outlier-prone, moderate-precision, high-temporal-resolution DEMs and produce a temporally consistent dataset of elevation changes.

In this study, we present a workflow designed to filter and interpolate elevation time series of high temporal resolution during surge events. We apply it to an unfiltered ASTER DEM dataset from Hugonnet et al. (2021). We use algorithms from the literature to filter outliers and interpolate elevations at monthly scale. We produce a regional dataset in the Karakoram region covering more than 100 surge-type glaciers. We assess the workflow performances, and we compare the outcome to other products and studies.

2 Data

In this study, we focus on the Karakoram region (Fig. 1). We use two existing surge-type glacier inventories that cover at least the period 2020 to 2020 in this region (Guillet et al., 2022; Guo et al., 2022). According to Guo et al. (2022) which considers glaciers larger than 0.4 km^2, there are 354 surge-type glaciers (individualizing tributaries) in the Karakoram and 128 probable or possible ones, representing about 8.6% of the regional number of glaciers (39.5% in term of area). Guillet et al. (2022) identified 223 surge-type glaciers on glaciers larger than 5 km^2 (not individualizing tributaries). These studies indicate that surge-type glaciers represents 39% to 45% of the glacierized area in this region.

We use the DEMs produced in the global study of Hugonnet et al. (2021), which ranged from 07/2000 to 09/2019 in this region. They are generated from satellite images of the ASTER sensor. They have been processed at 30 m resolution with the MMASTER workflow, running under the open-source photogrammetric library MicMac (Girod et al., 2017; Rupnik et al., 2017). They are stacked in time on the same spatial grid, and we use the "Elevation time stack" product at 100 m spatial resolution (see Extended Data Fig. 1, Hugonnet et al. (2021)). All DEMs with a root-mean-square-error of the elevation difference with TanDEM-X on ice-free terrain above 20 m have been removed (Hugonnet et al., 2021; Rizzoli et al., 2017). We use all ASTER elevations produced by MicMac for any stereo-correlation score, with lower correlation being associated to higher uncertainty (Hugonnet et al., 2021). As an exception, we identify erroneous correlation scores of exactly 51%, likely due to a processing peculiarity in MicMac to compute this score, and remove their associated elevations for the rest of the analysis.

Each stack extends over a 1x1 degree tile and is coregistered over TanDEM-X DEM. Each DEM is generated from three consecutive ASTER granules and co-registered independently. The sliding of granules processing regularly results in several DEMs per date.

https://doi.org/10.5194/egusphere-2024-3480
Preprint. Discussion started: 6 December 2024

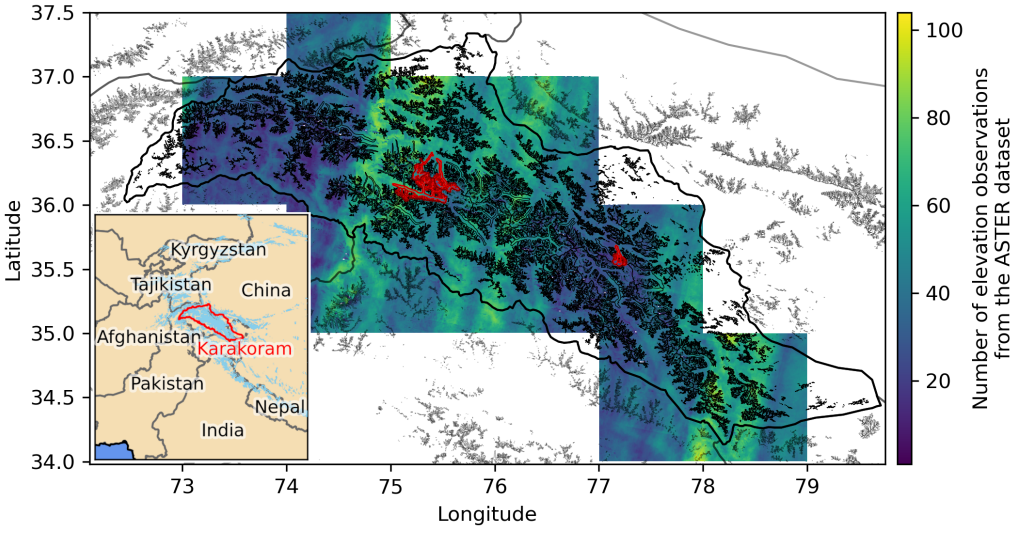

Figure 1. Main map focusing on the study area in the Karakoram, with regional localisation provided in the inset map. The colour scale shows the number of pre-filtered ASTER-derived elevation observations over the period 2000-2019 from Hugonnet et al. (2021). Glacier outlines from RGI7 are shown in dark tones. Glaciers outlined in red are, from West to East: Hispar, Yazghil, Khurdopin and Kyagar glaciers. The longitude and latitude are expressed in the coordinate reference system EPSG:4326 (WGS84).

The temporal sampling is heterogeneous in time and space (Fig. 1). Overall, 50% of consecutive on-glacier elevations are below 50 days apart, and about 90% are less than nine months apart. Said differently, 40% (75%, respectively) of the dates in the time series periods are between unfiltered observations which are less than six month apart (a year, respectively) (Fig. 2, solid orange line).

We use the Copernicus DEM GLO-90 as a reference elevation for coarse filtering of very large outliers (European Space Agency and Airbus, 2022). It is edited from the data of the TanDEM-X mission between 2011 and 2015. The impact of radar penetration is negligible compared to the threshold used (hundreds of metres).

3 Methods

3.1 General workflow

We aim to develop a workflow to filter and interpolate stacks of ASTER DEMs, specifically designed to handle surge events. We use the workflow of Hugonnet et al. (2021) as a baseline to which we compare our own workflow. It is noteworthy that Hugonnet et al. (2021) handled the same ASTER DEMs, but it was not specifically designed for surge type glacier elevation changes. Our workflow is divided into three main sections to get different levels of products (Fig. 3).
First, we implement two pre-filtering steps:

https://doi.org/10.5194/egusphere-2024-3480
Preprint. Discussion started: 6 December 2024

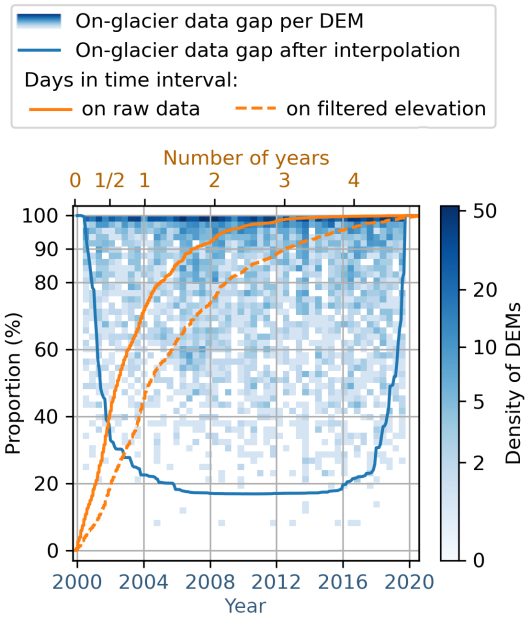

Figure 2. Data gap and temporal coverage of the time series at different processing level. In blue, the proportion of the on-glacier data gap per date, before and after the processing workflow. In orange, the proportion of days that fall below the time interval range (e.g., nearly 75% of any date in the time series periods are between unfiltered observations less than a year apart). The x-axis are independent, the y-axis is shared.

1. Spatial filter: we filter out pixels with a difference of more than 400 m between the ASTER DEM and GLO-90 reference DEM.

2. Merging of strips: we merge the DEM strips on the same day by keeping, at the pixel level, the elevation with the highest correlation score at overlaps.

Second, we filter the dataset to remove remaining outliers by three steps:

1. LOWESS workflow, core step of the filtering: we apply a LOWESS workflow (detailed in subsection 3.2) to remove pixels that are not consistent with temporally close observations in the time series.

2. Morphological 3x3 erosion: we implement a morphological erosion with a 3x3 kernel on the binary data mask. The ASTER elevation errors of this dataset are often correlated spatially to their neighbours. Removing the pixels directly around data gaps removes further outliers.

3. Removal of time series with less than 10 points: we consider such time series not dense enough for our application.

Third and finally, regular temporal interpolation with ALPS-REML: we interpolate the time series with a B-spline method with an automatic hyperparametrisation. We develop it in subsection 3.3. The interpolated elevations are provided as a monthly time series.

https://doi.org/10.5194/egusphere-2024-3480
Preprint. Discussion started: 6 December 2024

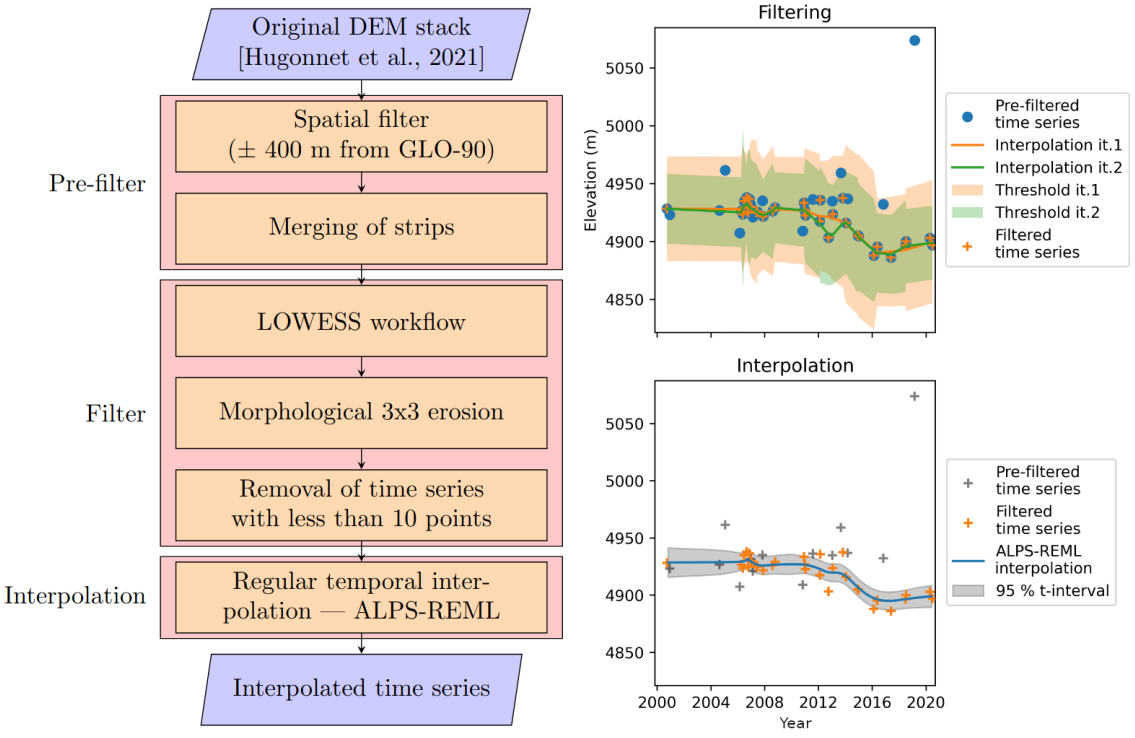

Figure 3. The complete workflow of the elevation time series processing, with an example of time series processed. Abbreviations: "it." ~iteration, "TS" ~time series.

3.2 LOWESS filter

The pre-filtering step is very coarse and excludes only the largest outliers. We thus additionally filter the elevation time series using the Locally Weighted Regression and Smoothing Scatterplots (LOWESS) algorithm in a sequence detailed later (Cleveland and Devlin, 1988; Derkacheva et al., 2020). It is a non-parametric, moving weighted regression. We use the Python *scikit-misc* implementation. For our dataset, the output of the regression is to sensitive to noise overall and too smooth over surges to be used directly as an interpolation of the elevation, so we use it for filtering only.

Here are the main parameters that have been tuned manually (Fig. 4):

- span: it is the smoothing parameter, expressed as the fraction [0-1] of points of the time series used at each local regression. A larger value implies more smoothing. We set it at 0.4 and 0.3 for the two iterations, respectively.
- degree: degree of the local polynomial regression. We choose a degree 2.
- family: assumed distribution of the errors, with a choice between "gaussian" (fit is performed with a least-squares) and "symmetric" (fit is performed robustly by redescending M-estimators). We use "symmetric".

https://doi.org/10.5194/egusphere-2024-3480
Preprint. Discussion started: 6 December 2024

- weights: weights to be given to individual observations in the sum of squared residuals. We use the uncertainty provided for each elevation in Hugonnet et al. (2021), which models heteroscedasticity (variable error) as a function of slope and the quality of stereo-correlation based on elevation differences on stable terrain (Hugonnet et al., 2022).

We use the LOWESS algorithm in the following sequence (Fig. 5): we run two iterations of the LOWESS regression with a decreasing smoothing factor. At each iteration, we compute a threshold envelope around the regression which is used to remove points falling outside of it. The envelopes are derivative-varying to prevent the filtering from removing true signals close to surge events. For the two consecutive iterations of outlier removal, respectively (plot in Fig. 5): the threshold to the regression ranges from 30 m width (resp. 45 m) at 0 m yr^{-1} derivative (constant elevation) to 100 m (resp. 150 m) at 50 m yr^{-1} derivative (assumed to be a potential surge signal). The worst time series have large temporal data gaps which can create computational errors for small smoothing parameters. Therefore, at each regression, we implement a step-by-step increase in the smoothing parameter in case of such errors, depicted as the faction value in Fig. 5. In case of computational error remaining after a +0.05 (resp. +0.10) increase of the fraction parameter, we filter out the full time series.

3.3 ALPS - REML interpolation

ALPS or Approximation by Localized Penalized Splines is a unified time series modeling framework introduced in Shekhar et al. (2021). ALPS builds on the localized nature of B-spline basis functions to model time series with highly non-uniform sampling, thereby improving the state of the art in this domain. In this research, we use a mixed modeling analog of the statistical B-spline regression model introduced in Shekhar et al. (2021). This is motivated from the capability of the mixed models to segregate high frequency and low frequency components of the overall model, thus allowing us to narrow down the effect of the regularization/smoothing specifically on the high frequency components that drive the overfitting behavior.

Another change inherent in our approach as compared to the approach described in Shekhar et al. (2021) is the model fitting algorithm. As described in Shekhar et al. (2021), the original ALPS model used the Generalized Cross Validation (GCV) metric for estimating the model parameters. However, here we take an alternative route and use the restricted maximum likelihood (REML) approach for fitting our model. GCV metric quantifies the generalization error of model by predicting at data points, not used for fitting the regression model. And hence, minimization of GCV metric forces the model to predict accurately at unseen locations as described in Wahba (1990). REML on the other hand formulates the problem from a statistical perspective and optimizes the regression parameters such that the probability of observing the data is maximized. A more detailed explaination of REML can be found in Ruppert et al. (2009). The reason for choosing REML over GCV in this work can be attributed to the fact that GCV is well known to under-estimate model uncertainty, thereby providing over-confident prediction which in some extreme cases can be misleading. Additionally, for the time series under consideration in this work, ALPS model with original GCV based model fitting was overfitting to noise, making it unsuitable. In order to produce interpolated results in this paper, we use the same ALPS-REML code. We however set a degree of the basis functions p of 4, and an order of penalty q of 1.

https://doi.org/10.5194/egusphere-2024-3480
Preprint. Discussion started: 6 December 2024

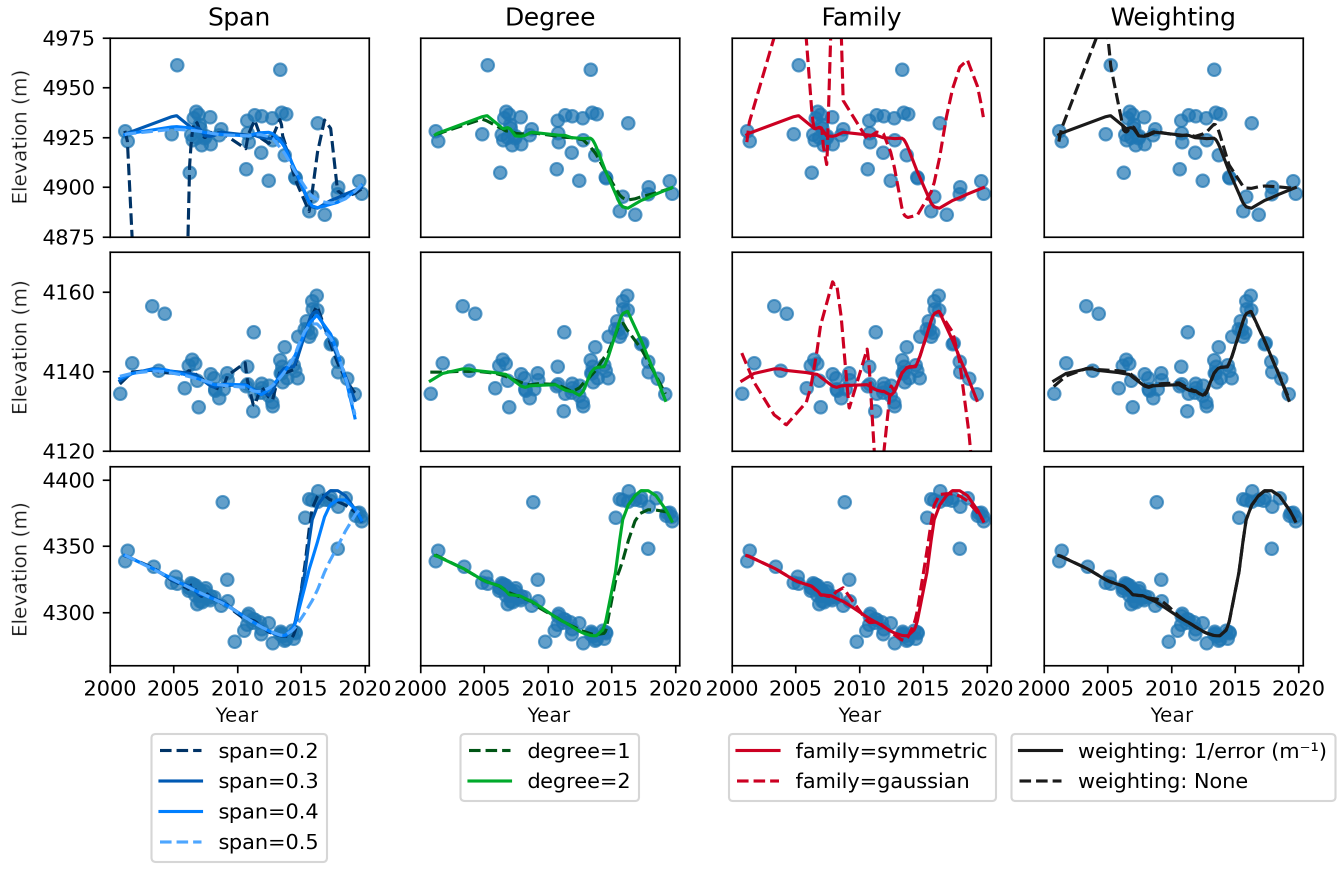

Figure 4. Impacts of the different LOWESS parameters on the filtered time series. Each column corresponds to the different LOWESS results for different values of each of the four main parameter. Plain lines are the final selected values. The line corresponds to three different data points (locations shown on Fig. 7.c).

We compare extensively Gaussian Process Regression (GP regression) and ALPS-REML in our study. GP regression is a non-parametric method, for which we can define a kernel with mathematical functions that fit the prior belief of the phenomenon to model (e.g., periodicity, linear trend...). It is the method used by Hugonnet et al. (2021) on this same dataset, to compute long-term mass balance estimations worldwide. GP regression is more complex to use, as it requires the definition of kernels based on variance analysis of the elevation changes. ALPS on the opposite approximate the data with polynomials, which does not relies on prior belief of the data.

3.4 Volume transfer estimate

We estimate the volume transferred during some surge events by assessing both the glacier net volume changes over specific areas. Unless specified, the extent is the surge-affected area manually drawn from the elevation change map at the surge timing.

https://doi.org/10.5194/egusphere-2024-3480
Preprint. Discussion started: 6 December 2024

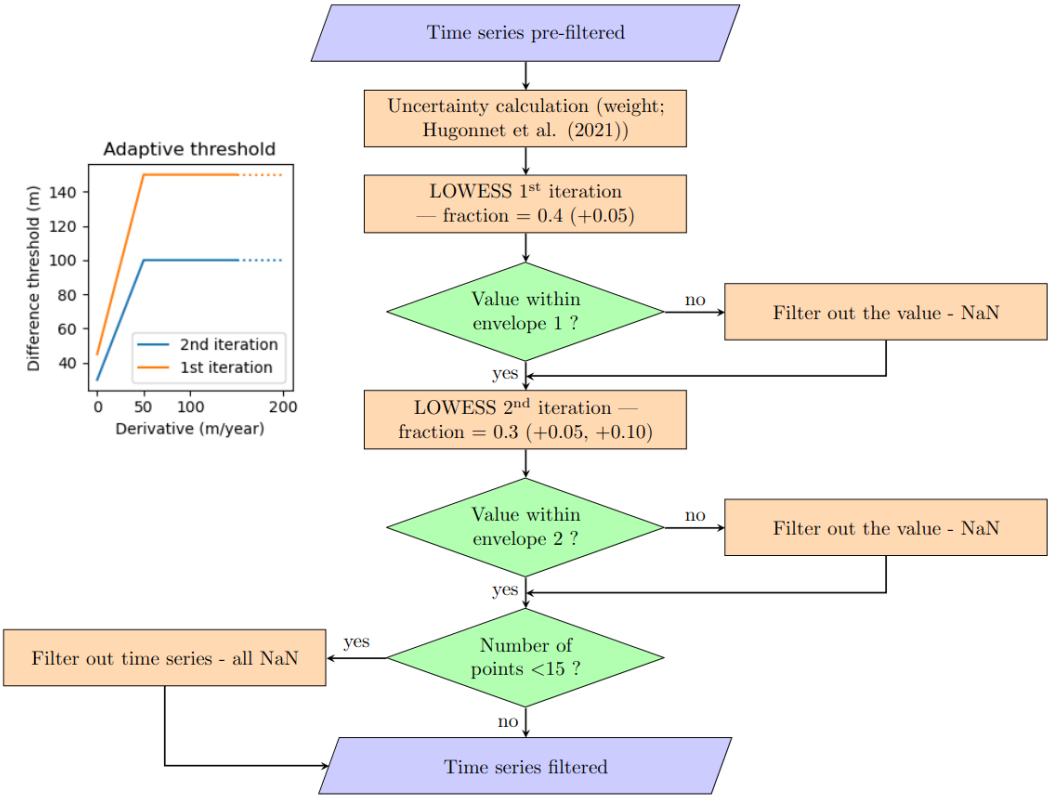

Figure 5. Complete workflow of the LOWESS filter step. The envelopes are the maximum distance threshold allowed between the LOWESS regression and the time series values, which vary with the LOWESS regression derivatives as shown in the inserted plot on the top-left.

We separate the reservoir and the receiving areas in two distinct polygons.

To compute the volume transferred, we differentiate the elevation at two dates. We then mask surrounding areas. We interpolate data gaps in the elevation change maps with a bilinear interpolation. Finally, the sum of elevation changes per area (reservoir or receiving area) are converted to volume via the size of pixels.

The sum between the volume changes in the two areas gives the volume imbalance. We divide the volume imbalance by the surge-affected area to provide the same indicator in metre. This metric imbalance is more representative of the corresponding uniform elevation change, and it permits to compare the results independently of the glacier size.

4 Results

4.1 Performance of the outlier filtering

We compare the filter and the temporal interpolation developed to those of Hugonnet et al. (2021) on locations that are affected by surges, but also for all the glaciers of the region (Fig. 6, Fig. 7). In Hugonnet et al. (2021), the iterative GP regression

https://doi.org/10.5194/egusphere-2024-3480
Preprint. Discussion started: 6 December 2024

filtering is responsible for removing some high-amplitude surge signals (Fig. 6.c1-2, or abnormal gap circled in red in Fig. 7.a). In Hugonnet et al. (2021), the kernel of the GP regression does not model well the change in elevation that is typically observed during surge events. The elevation change rate modelled for interpolation is much lower than surge ones, and the time length scale of the changes modelled is longer than most of the surge time-scales (e.g., Fig. 6.c1). Modifications of this kernel to allow for stronger changes in elevation have not proven to be efficient enough. In our workflow, the LOWESS filter behaves with varying performance, depending on the time series quality (noise, temporal density, surge amplitude). It does conserve nearly all known surge events in our study area and period, with one exception being surge events with strong melt before and after the surge. A typical example of this is a part of the front of the Khurdopin glacier (Fig. A2.a). In this time series, two critical observations are filtered out around 2017 during the short surge. Because of this, the ALPS-REML interpolation smooths the signal even further, as both LOWESS and ALPS fits are sensitive to the lack of elevation measurements at abrupt trend changes, with less point to constrain the fitting. Strong melt in the receiving area increases the elevation-change smoothing effect of the fits by reducing the average elevation change locally before and after the surge.

The LOWESS workflow is also sensitive to weight estimate and noise on unfavourable terrain (textureless and steep areas for example), resulting in more unrealistic erratic filtering than those of the original study (red circles in Fig. 7.b). This is often due to the correlation error that is not very representative of the actual pixel quality: outliers may have lower uncertainties than observations close to the true elevation (e.g., Fig. A2.e). These types of locations are not predominant in surge-affected areas, and a number of them are completely filtered out by the following steps of the filter. The filtered-out areas (data gaps) are more prevalent with our method, mostly over unfavourable terrain. No discontinuities caused by erroneous filtering are visible on Fig. 7.b, compared to a (red circle). We attribute this difference to the filtering with the LOWESS filter, that is more suited to preserve abrupt elevation change signal.

After filtering, nearly 40% (75%, respectively) of any date in the time series periods are between unfiltered observations less than a year (two years, respectively). Before pre-filtering and filtering, for the same percentage, it was a half-year (one year, respectively) (Fig. 2, solid orange line). The time series are about twice less dense than before, temporally.

4.2 Performance of the temporal interpolation

The interpolation of Hugonnet et al. (2021) is a GP regression with the same kernel as for the filtering. Fig. 6.a-b1 shows edge effects at the temporal bound of the time series due to the linear member of the kernel. The seasonal member of the kernel creates the undulations of a one-year length scale. In comparison, our workflow shows only limited border effects. It better fits changes in trends (ex. Fig 6.a1-2), and preserves most of the surge signal (Fig 6.c2). However, dense clusters of points are regularly over-fitted, creating wavelet artefacts spanning typically about 6 to 12 months, as illustrated in Fig. 6.c2 around 2006 and 2011 or 6.a2 around 2006. Comparing the final interpolated elevation changes over two years (Fig. 7.c-d), our workflow can capture the complete surge signal of Hispar and Braldu glaciers (red circles in Fig. 7.c), which was not the case for the previous workflow. At these locations, the original method of Hugonnet et al. (2021) removes completely the surge signal, filling the period with the global trend or a completely smoothed-out trend (e.g., Fig. A1). Moreover, several reservoir or receiving areas of the surges have weakest changes with the original method, which tend to smooth remaining surge signals,

https://doi.org/10.5194/egusphere-2024-3480
Preprint. Discussion started: 6 December 2024

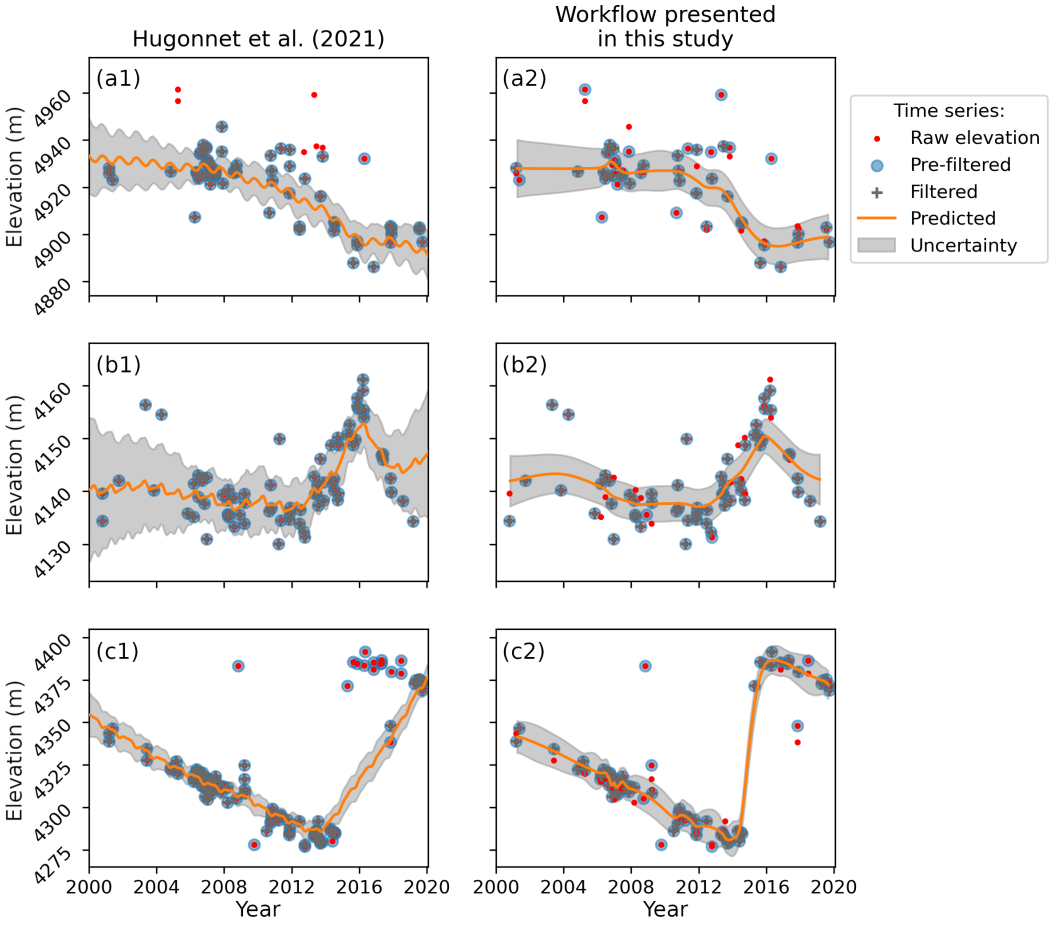

Figure 6. Comparison of pre-filter, filter and interpolation methods of the data's processing: (a1-c1) from Hugonnet et al. (2021) against (a2-c2) the workflow presented in this study. The three time series show all a surge around 2015, their location is represented on the map Fig. 7.c (points TSa-c). The uncertainty is the 1 σ standard deviation credible interval for GP regression (Hugonnet et al., 2021), and it is the 95% t-confidence interval for ALPS-REML (this workflow).

both in time and in elevation (e.g., Fig. 6.c1 and Fig. A2.d). The maximum on-glacier spatial coverage of interpolated elevation over Karakoram is about 80% from 2005 to 2015 (Fig. 2, solid blue line). Some glaciers are more affected by data gaps than others, in agreement with areas with a low number of observations (Fig. 1, e.g. Shisper glacier).

4.3 Analysis of selected surge events

To illustrate the outputs of our method, we analyse four surge events that have been studied in the literature. They occur on four glaciers: Hispar, Khurdopin, Kyagar and Yazghil glaciers. Fig. 8 shows the spatio-temporal evolution of the surface elevation

https://doi.org/10.5194/egusphere-2024-3480
Preprint. Discussion started: 6 December 2024

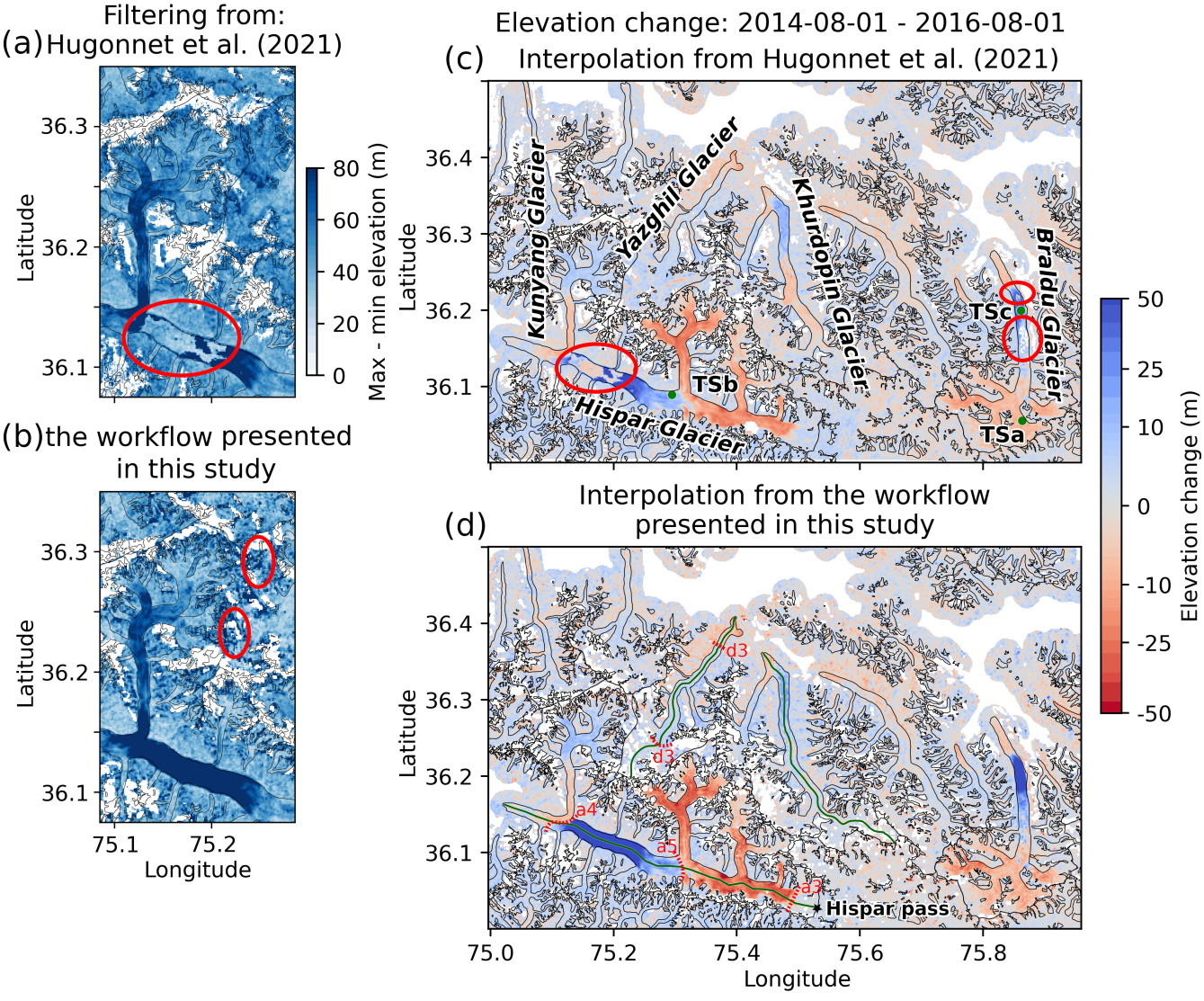

Figure 7. a-b: maps of maximum elevation change after the filter methods. c-d: elevation change maps over two years (Hispar glacier surge period). The green points and their labels (TSa-c) in c) correspond to the localisation of the time series in Fig. 6 (a-c). Their coordinates are (EPSG:4326): TSa (75.863, 36.055), TSb (75.295,36.089) and TSc (75.861,36.200). The green lines on d are the centerlines of the glaciers.

225 of the glaciers along their centerline (green line on Fig. 7).d, except for Kyagar glacier outside of the visible area of the map).

We observe the influence of Kunyang tributary surge that reached Hispar main glacier tongue (around kilometre 40) in early 2008 (Fig. 8.a, area a1). The surge front propagates downstream for several years with a decreasing speed (2009-2012, a1), while strong thinning starts at the junction and approximatively five kilometres upstream of the surge front. A slight and short

https://doi.org/10.5194/egusphere-2024-3480
Preprint. Discussion started: 6 December 2024

positive elevation change on the main trunk of Hispar up to a few hundred meters before the junction (around 49 km), starting one year after the surge reached the main trunk, may indicate mass accumulation from a blockage of the ice flow (Fig. 8.a, area a2). The time series (not presented here) confirms this thickness gain. Meanwhile, a slight and more regular buildup or thickening occurs above, upslope of 25 km (Fig. 8.a, area a6). The Hispar surge of the main trunk seems to start in early to mid-2014 and end mid-2016 (area between the lines a3 and a4 on Fig. 7.d and Fig. 8), with small mass displacement until the end of 2017, downslope of the Kunyang junction. Sharp wavelets of positive and negative elevation changes occur from mid-2013 to mid-2014, which we attribute to artefacts of our method, are visible horizontally on Fig. 8.a. The time series shows dense and very scattered elevation observations at this period even on stable ground (Fig. A2.c), causing these artefacts. This may be due to tilts or undulations remaining in the DEMs. The results indicate that the dynamic balance line location is not stable in time. On the branch of the Hispar Pass (source of one of the main branches, location on Fig. 7.d), the reservoir area extends from 5 km from the pass, at an icefall (line a3 on Fig. 7.d and Fig. 8), down to 20 km from the pass at the junction with the Yutmaru tributary in the first part of the surge. From the end of 2015 to the end of the surge, it then extends 5-10 more kilometres down (below the junction) (line a5 on Fig. 7.d and Fig. 8). We plot an elevation time series at this location (Fig. 6.b2, location TSb on Fig. 7.c). The receiving area extends from the end of the reservoir area at 20-25 km from the pass along centerline, down to nearly 40 km from the pass at the junction with the Kunyang tributary (line a4 on Fig. 7.d and Fig. 8.a). We now assess the volume of ice transferred during the surge, from 2014-01-01 to 2016-09-01. We calculate a volume change over the reservoir area of -2411 $x10^6$ m^3, and of 3110 $x10^6$ m^3 over the receiving area (Table 1). The imbalance resulting is of 700 $x10^6$ m^3, which represents an evenly distributed layer of 4.55 m thick over the whole surge-affected area. The difference between volume gain and loss, or imbalance, is unexpected as the surge occurs over a short time period and mass should be roughly conserved. The imbalance is quite similar when using two filtered ASTER DEMs over a similar period over this surge, instead of interpolated.

Khurdopin glacier has a gradual surge onset or pre-surge phase, visible like a gradual positive elevation change slowly propagating downward as a kinematic wave (Fig. 8.b, area b1). The "build-up front" or kinematic wave extends from about 27 km of the glacier source in 2002 to about 33 km in 2015, representing a regular advance of about 460 m per year, which is approximately 6 times faster than the surface velocity, according to the NASA MEaSUREs ITS_LIVE project repository (Gardner et al., 2022). The upper limit of the build-up area and then of the reservoir area is stable in time, at the bottom of an icefall. The actual surge starts in 2016, continuing the kinematic wave as a surge front. Both our filter and interpolation methods here fail to capture fully the surge signal of the receiving area (see discussion section 5.2). It leads to an apparent surge end in early-2019 on interpolated data, which is overestimated by about a year and half according to non-interpolated time series (Fig. A2.a). A distinct and local positive elevation change pattern is visible after the surge around kilometre 23 (Fig. 8.b, area b2).

Kyagar glacier is located about 110 km to the East of the other glaciers (Fig. 1). A slight mass buildup is visible since the beginning of the time series in the first ten kilometres of the glacier, and extends up to about 14 km a few years before the surge. It starts around the end of 2013 or the start of 2014, and ends in late 2015. The beginning of the surge appears sooner

https://doi.org/10.5194/egusphere-2024-3480
Preprint. Discussion started: 6 December 2024

in the interpolated time series, and the end is also represented nearly a year later from what is visible on the non-interpolated time series of most of the receiving area. During the surge period, there are about 1-2 observations per year. There is an area where the ASTER time series is of bad quality resulting in some artefacts after processing, at 5 km from the glacier source, which is located around the equilibrium line of the glacier. The reservoir area seems to extends upward of this area. This issue biases the volume transfer calculation. We manually draw a mask to remove artefacts for a better estimate (Table 1).

Our dataset captures a full cycle of Yazghil glacier. On this glacier, the surge signal has a low amplitude (approximately ten metres) compared to the time series, and thus noise is often overfitted. This results in frequent interpolation artefacts (horizontal lines on Fig. 8.d). A surge starts in late 2003 and ends in late 2006 or early 2007 (Fig. 8.d, area d1), and a new surge starts in 2017 or early 2018 (the end is not captured; 8.d area d2). One of the tributaries of Yazghil glacier (junction at km 18) is also surge-type, and seems to have surged during our study period in about 2008-2013. The buildup and emptying of the first surge seems weaker than the second one, and extends less up-glacier of the junction, compared to the second surge (Fig. 8.d area d3, delimited by dotted lines d3 on Fig. 7.d). This may be related to the effect of the tributary surge, that stopped at the junction but could have yet increased mass input by a blocking effect.

https://doi.org/10.5194/egusphere-2024-3480
Preprint. Discussion started: 6 December 2024

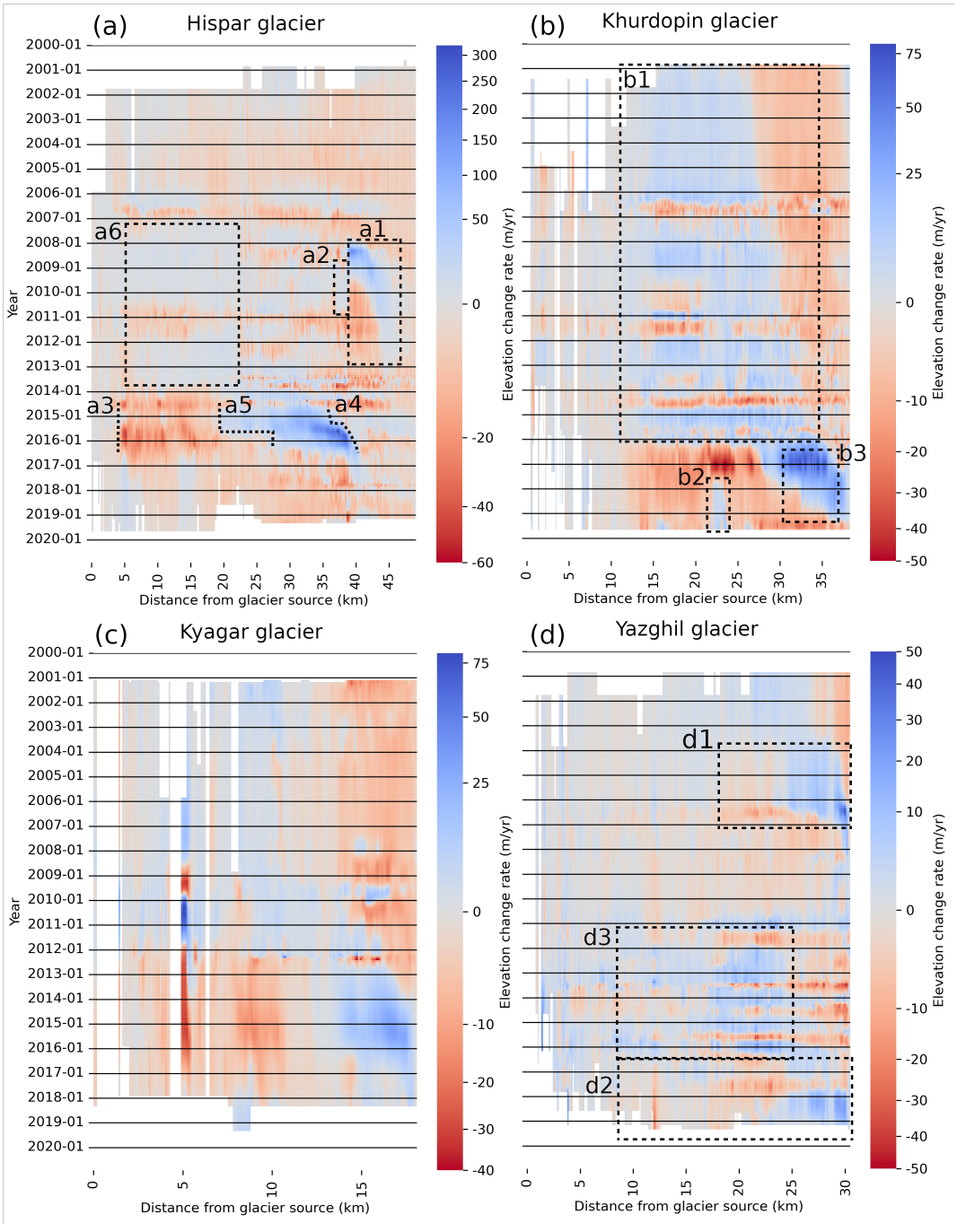

Figure 8. a-d: Hovmöller diagrams, spatio-temporal evolution of the interpolated surface elevation of four glaciers. The elevation change is sampled on the centerline of the glacier (in green in Fig. 7.d). Glaciers flow from left to right on the different panels. Note that the colorscales represent different elevation change rate amplitude and that they are non linear.

https://doi.org/10.5194/egusphere-2024-3480
Preprint. Discussion started: 6 December 2024

Glacier RGI 7.0 code	Date start [time series]	Date end [time series]	Reservoir vol. change	Receiving vol. change	Imbalance	Data gap [after interp.]
Hispar 21670	2014-01 [2014-05]	2016-09 [2016-06]	-2411 x 10^6 m^3	3110 x 10^6 m^3	700 x 10^6 m^3 4.55 m	0.6% [0.2%]
Yazghil 21865	2003-07 [2004-01]	2007-01 [2006-08]	-32 x 10^6 m^3	63 x 10^6 m^3	-31 x 10^6 m^3 -2.19 m	0% [0%]
Khurdopin 14958	2016-03 [2016-04]	2019-03 [2017-07]	-801 x 10^6 m^3	711 x 10^6 m^3	-90 x 10^6 m^3 -1.9 m	1.4% [0.8%]
Kyagar 14958	2012-11 [2013-11]	2017-01 [2015-12]	-271 x 10^6 m^3	267 x 10^6 m^3	-4 x 10^6 m^3 -0.12 m	2.4% [0.2%]
Kyagar without artefact	—	—	-228 x 10^6 m^3	267 x 10^6 m^3	39 x 10^6 m^3 1.33 m	5.6% [0.2%]

Table 1. Timing and volume transferred of surges for four glaciers in the study area. The main dates are given according to the Hovmöller diagrams on interpolated changes (Figure 8). We compute the volume transferred ("vol. change") from interpolated DEMs at these dates to capture the corresponding volume change from both reservoir and receiving areas. The dates between brackets are those estimated visually on non-interpolated time series, thus less smoothed, given for indication. They are not accurate to the month due to ASTER acquisition dates. Volume changes are in x10^6 m^3. The volume change and the imbalance computation method is detailed in the subsection 3.4. The data gap is given in percentage of the surge-affected area. The percentage between brackets is the data gap proportion remaining after a bilinear interpolation of the elevation change. The prefix of RGI codes is "RGI2000-v7.0-G-14-".

5 Discussion

5.1 Processing quality

The uncertainty estimate of the ALPS-REML algorithm cannot represent the ability of the filter to keep true elevations and remove outliers. To assess the quality of our results, we 1) compare our interpolated elevations with external DEMs produced from high resolution satellite imagery, and 2) test the sensitivity of the interpolation to data gaps.

First, we compare the interpolated elevation with external DEMs, produced from optical very-high resolution satellite imagery (Fig. 9). This comparison provides a validation of estimated elevation during a few surge events. We use SPOT5 HRS and SPOT6 DEMs generated by Berthier and Brun (2019), and along-track HMA DEMs (Shean, 2017). We co-register each external DEM on the ASTER interpolation. The NMAD score on stable terrain after co-registration ranges from 6.8 to 15.6 m (median 7.4 m), which shows a good agreement with discrepancies of a few meters. Extreme cases occur locally with differences reaching tens of meters, but it is generally unclear which dataset is flawed. The case study of Khurdopin glacier surge, discussed above, shows however that a discrepancy of a hundred meters is credible on exceptional events. The map of elevation

https://doi.org/10.5194/egusphere-2024-3480
Preprint. Discussion started: 6 December 2024

differences shows moderate differences overall, which can be important locally (Fig. 10). Systematic differences appear over the whole glaciers: e.g., the median difference is of -4.3 m (standard deviation of 9.7 m) on Hispar glacier on 2015-10-13, -5.2 m (standard deviation of 8.7) on Braldu glacier on 2015-11-28. Larger local differences are located around the surge front: e.g., up to 24 m at Hispar surge front on 2015-10-13. We compute the percentile of elevation change values during a surge event and during quiescence (Table 2). The results do not show important difference at the scale of the surge-affected area. The discrepancy associated to a surge period is overall of the same magnitude as other noise, considering the large standard deviations.

Percentile:	2^{nd}	10^{th}	50^{th} (median)	90^{th}	90^{th}
During surge	-17.3 m (SD 12.0 m)	-7.5 m (SD 5.9 m)	-0.1 m (SD 3.6 m)	13.8 m (SD 13.6 m)	28.7 m (SD 29.6 m)
Quiescence	-16.2 m (SD 9.3 m)	-8.5 m (SD 5.1 m)	-2.1 m (SD 3.8 m)	3.5 m (SD 3.2 m)	11.4 m (SD 6.1 m)

Table 2. Average percentiles of elevation difference between reference DEMs and interpolated ASTER DEMs. We compute independently the percentile over each surge-affected area of Hispar glacier, of Kunyang glacier (Hispar glacier tributary) and of Braldu glacier. We then get the average of the percentiles according to the surge phases of the glaciers. *SD* are standard deviations. There are four reference DEM per surge phase: SPOT5, SPOT6 and 2x HMA DEM during surges; 3x SPOT 5 and SPOT6 in quiescence phase.

One of the main limitations of our results is the relatively sparse observations in the time domain. Here we investigate the impact of data gaps on our interpolated time series. The spatial data gap on-glacier at the regional scale is nearly 20% at best over our study area, during 11 years (from 2005 to 2016). It rises to 40% of data gap to capture five more years (Fig. 2). A number of surge events are interpolated from temporally low-density time series (e.g. less than 3 observations per year) or thus with large data gaps, mostly clustered over specific Karakoram parts (Fig. 1, e.g. Shisper glacier). In such situations, our method of filtering and interpolation usually leads to an underestimate of the volume transferred and an overestimate of the surge duration (e.g., twice its duration for the Kyagar glacier), even when relying on the filtered time series and not on the interpolated one. Onset and end dates cannot be precise to a few months for a surging area with only one or two observations per year (e.g., the case study of the Kyagar glacier surge). To test the sensitivity of the ALPS-REML method to data gap, we interpolate an elevation time series after removing all points in a 450-day moving window (Fig. 11). Each iteration results in a period of at least 450 days without observation. For the selected time series a) and c), the test shows strong smoothing, although the surge signal is still visible over large time frames. The interpolated dates of the surge onset (ending, respectively) are advanced (delayed, respectively) up to two years compared to the original interpolation. The surge elevation change can be underestimated up to about 20 meters. This can be larger for larger time gaps or surges with stronger elevation changes before or after the surge. Case b) is specific, as it lies close to the dynamic balance line (in the receiving area at an early stage of the surge, and then in the reservoir area). The surge signal is completely smoothed out when the data gaps occur in the middle of the surge. Other specific cases of surges, with limited elevation changes but with strong melt or strong buildups before or after the surge, could be prone to the same problem. An ASTER dataset generated with smaller noises and errors could improve the interpolated dataset ability to capture surges.

https://doi.org/10.5194/egusphere-2024-3480
Preprint. Discussion started: 6 December 2024

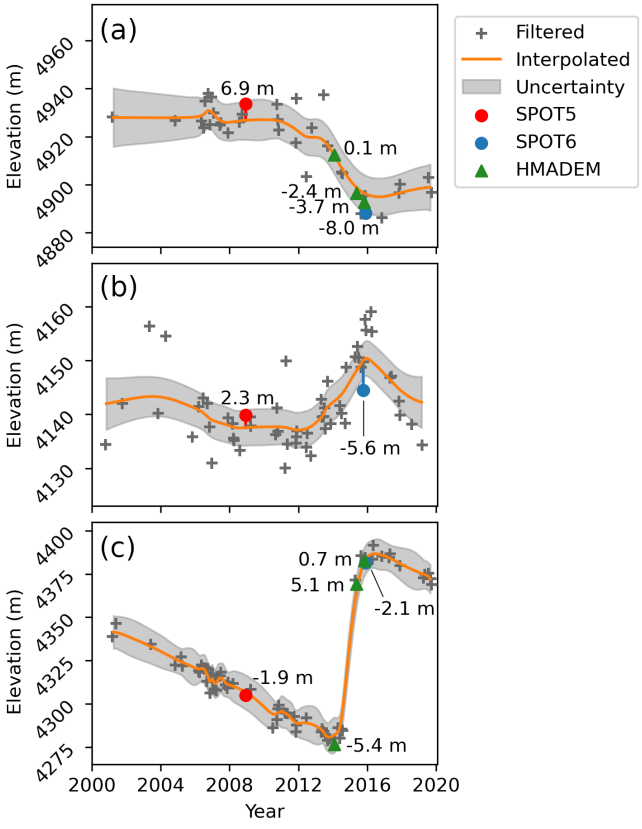

Figure 9. a-c: comparison of elevation between SPOT DEMs (SPOT5 HRS and SPOT6) and HMA DEMs against ASTER elevations interpolated at the same dates.

5.2 Comparison of surge characteristics with the literature

Regarding the surge of the main trunk of Hispar described in the section 4.3, our date estimates (mid-2014 to mid-2016) are very close to the date estimated in previous studies (autumn 2014 to mid-2016), which were based on remotely sensed velocities (Paul et al., 2017; Guo et al., 2020). Paul et al. (2017) notices a 6-month stop of the surge front around 35 km, up to mid-2015: it is slightly visible here at similar time (Fig. 8.a, line a4). The fact the reservoir area does not extends above the icefall has already been observed on other glaciers, including Khurdopin in our study (Nolan et al., 2021; Echelmeyer et al., 1987). This can be due to the lower drawdown that the kinematic disconnection the icefall creates (Nolan et al., 2021; Terleth et al., 2021). The displacement of the dynamic balance line of this surge has not been mentioned in other studies. Velocity data is probably not able to capture such change, which is certainly only visible with elevation change data at short timescale. Bhambri et al. (2022) estimate volume changes over the period 2014-2020 from ASTER DEMs of -2785 x10^6 m^3 in the reservoir area, and 2581.6 $\pm$ 465 x10^6 m^3 in the receiving area. Our estimates over the surge dates are similar for the reservoir area volume change, -2411 x10^6 m^3 (about 13% difference; Table 1). We find a larger difference in the receiving area, with

https://doi.org/10.5194/egusphere-2024-3480
Preprint. Discussion started: 6 December 2024

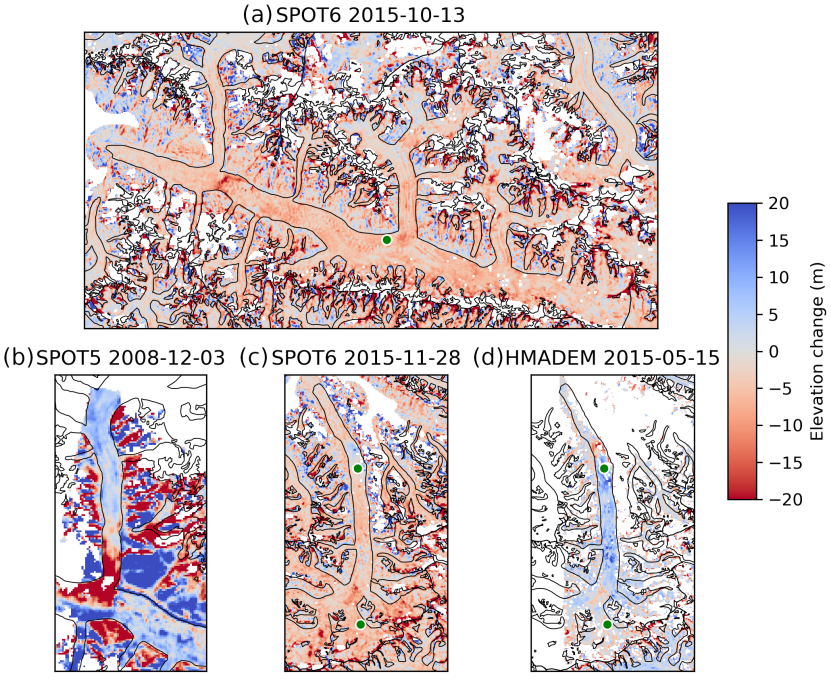

Figure 10. a-d: difference of elevation between SPOT DEMs (SPOT5 HRS and SPOT6) and HMA DEMs against ASTER elevations interpolated at the same dates. The areas selected are the Hispar glacier (surge in 2014-2016), its Kunyang tributary (surge in 2007-2008), and two over the Braldu glacier (surge in 2013-2016). The panels have the same colour range. The green dots show sampled time series (Fig. 6, 7.c and 9).

3110 x10^6 m^3 (20%), for which post-surge melt of the deposited ice volume during three or four years likely partially explain the smaller volume of Bhambri et al. (2022). Accordingly, we can extend our period up to mid-2018 before large data gaps appears in our time series. From 2014-01 to 2018-08, the volume change estimate is closer to their result: -2736 / 2793 x10^6 m^3 (2% and 8% difference, respectively). The impact of crevasse opening on the apparent surface elevation have not been assessed.

The gradual surge onset we observe for Khurdopin glacier corresponds to the observations of several studies (Steiner et al., 2018; Imran and Ahmad, 2021). The propagation of the pre-surge thickening front or kinematic wave have however not been observed on this glacier. The existence of kinematic wave propagating the surge front have regularly been observed on other surges (e.g., Turrin et al., 2013; Kotlyakov et al., 2018; Cuffey and Paterson, 2010). Turrin et al. (2013) observed on velocity data the propagation of a kinematic wave several years before the Bering glacier surge, triggered consecutively to the passage of the wave down the reservoir area. This wave also propagated faster than the surface velocity. There is several similarities to what we observe on Khurdopin glacier. The surge started in October 2016 according to Imran and Ahmad (2021), a bit later than our spring 2016 estimate (Table 1). Steiner et al. (2018) estimate the volume received in the receiving area at 1182 x10^6 m^3 during late August 2015 (elevation extrapolated linearly from TanDEM-X in 2011) to May 2017 (ASTER) data, after

https://doi.org/10.5194/egusphere-2024-3480
Preprint. Discussion started: 6 December 2024

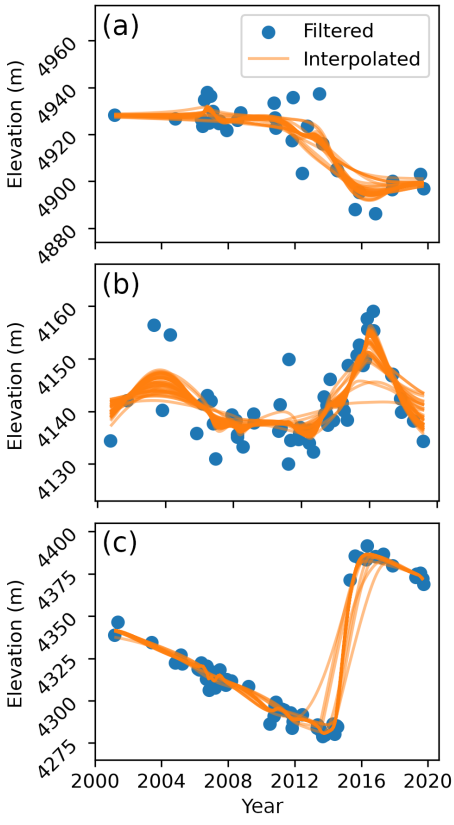

Figure 11. a-c: test of interpolation robustness. For the three selected time series of Fig. 6, we remove points during 450 continuous days over a moving window for which each interpolation is in orange.

reassessment of the estimate (Jakob Steiner, personal communication). Our estimate over 2015-09-01 to 2017-06-01 is 425 x10^6 m^3. However, both our filter and interpolation methods here fail to capture fully the surge signal of the receiving area, in the lower part of the glacier (Fig. 8.b area b3). This is due to point density combined with a strong thinning signal after the surge (Fig. A2.a). The filter workflow did remove some of the 2-3 DEM acquisitions over 2017 and 2018 with credible values. May 2017 is the month with the largest difference between the DEM observations and the interpolation, with up to about 100 m of elevation change underestimation compared with the pre-filtered data. Over such areas, the apparent surge signal duration after interpolation is about 3 years instead of less than 1 year, and may miss locally a maximum of 40 m (about 30%) of the total elevation change over these three years. Our estimate of the volume transferred in Table 1 is thus underestimated in the receiving area. The difference of pre-filtered DEMs from 2015-08-20 to 2017-05-21 shows a cumulative positive mass change of 648 x10^6 m^3. It is 152% more than with the interpolation, still nearly half of the estimate of Steiner et al. (2018) which may be also partially overestimated due to their linear extrapolation as the gradual surge onset extends further down-glacier from the 2000-2011 trend. The maximum thickness gain noted by Steiner et al. (2018) was 160 m over this period, against 122 m with our pre-filtered DEMs (70 m on interpolated DEMs). The case of this surge shows that our workflow may be inefficient

https://doi.org/10.5194/egusphere-2024-3480
Preprint. Discussion started: 6 December 2024

to preserve surge signal, in the case of a low number of DEMs available, aggravated by strong thinning out of the surge period.

Kyagar glacier is located in an area of poor ASTER coverage, compared to other selected glaciers (Fig. 1). During the surge period, there are about 1-2 observations per year, which leads the interpolation to smooth the surge signal. Thus, the onset and ending are visible around end-2012 and early-2017 on interpolated data, while non-interpolated time series leads to the more restricted end-2013 to end-2015 estimates. Round et al. (2017) uses satellite imagery to compute velocities and describe precisely the surge development. They find a surge onset in May 2014 after a pre-surge acceleration of 2.5 years, and a surge end between July and August 2015 with limited deceleration later. Li et al. (2023) find very similar timings, plus a continuing deceleration in 2016-2019. Gao et al. (2024) report similar timing, although considering a re-acceleration in 2016 as part of the surge. Gao et al. (2024) estimated the volume transported from ASTER DEMs. Over July 2012 to December 2017, they estimate the received volume at 321 $\pm$ 12 x10^6 m^3, against 260 x10^6 m^3 with our interpolated data. Their reservoir area volume change estimate is -383 $\pm$ 30 x10^6 m^3, against -328 x10^6 m^3 for our dataset over the same dates and approximative area (-285 x10^6 m^3 with bilinear interpolation of the artefact area). It represents differences in volume transferred estimate of 19% and 14%. The study states a glacier mass balance of 0.26 $\pm$ 0.02 m w.e. a^{-1} over the same period. After hypsometric interpolation, we find -0.26 m w.e. a^{-1}, 0.01 m w.e. a^{-1} after manual removal of artefacts.

Yazghil glacier has not been extensively researched. Bhambri et al. (2017) date the surge in 2006, with a gradual increase of velocities before this year. The study estimate from 1972-2016 data that the Yazghil glacier has a cycle length (surge repetition period, including quiescence and surge durations) of about 8 years, one of the shortest surge cycles in HMA. The next surge, which was expected to occur around 2014 based on the cycle length, had not started by the end of 2016, according to the study. Our data suggest it started 1-2 years later, implying a longer quiescence phase of 11-13 years. We described in section 4.3 a possible blocking effect with mass buildup created by the surge of a tributary. In addition to the case of Hispar and Kunyang glaciers described above, some blocking effects suspected here have already been observed in this region (Paul, 2015).

Overall, the dataset produced by our workflow compares well with the existing observations from the literature. The surge dates and the estimated volume transferred are in agreement, except for the dating of the Kyagar surge and the transferred volume estimate of the Khurdopin surge (Table 1). The order of magnitude of the imbalances corresponds to the order of magnitude of the measurement uncertainty. For the two critical cases (Kyagar and Khurdopin surges), the limit of the workflow occurs in case of a low number of DEMs, worsened in the case of a strong thinning signal out of the surge period (Khurdopin surge). Our dataset offers new insights on some undescribed processes in these studies, such as the displacement of the dynamic balance line of the Hispar surge or the propagation of a pre-surge bulge front of the Khurdopin surge.

5.3 Elevation change comparison

We assess the difference in elevation change estimate between the processing workflow from Hugonnet et al. (2021) and this workflow. Previous figures showed local differences, here we compare the elevation changes of pixels belonging to eight surge

https://doi.org/10.5194/egusphere-2024-3480
Preprint. Discussion started: 6 December 2024

events (Fig. 12, individual graphs in appendix Fig. C1). We observe strong smoothing of the original dataset cutting out surge signals in receiving areas (with positive elevation changes), that are better interpolated by our workflow (Fig. 12 zone A). There is no symmetric pattern for negative changes in reservoir areas, probably because of the smaller rates of elevation changes. It is mostly representative of surges with important and rapid elevation changes: surges of the Hispar, Braldu and Kunyang glaciers (Fig. C1), and to a lesser extent Khurdopin glacier surge. For such glaciers, major differences in total volume change are expected. This is clear in the volumes transferred estimates from the original dataset of Hugonnet et al. (2021) on Hispar and Khurdopin glacier surges (Fig. B1). Other glaciers also have smaller estimated volumes than with our method, but with smaller discrepancies. Compared with Hugonnet et al. (2021), our method finds larger absolute rates of elevations changes (pattern B on Figure 12), probably due to the stronger smoothing of Hugonnet et al. (2021) (e.g., Fig. 6.a1 or Fig. A2.d). Our method creates some artefacts, especially in the accumulation area where elevation changes are close to zero (zone C on figure 12). This is the case for Kyagar and Braldu glacier surges (Fig. C1).

This figure also illustrates non-uniform elevation change patterns common to all the surges here (Fig. 12). The elevation changes are much larger in the receiving area, whether the glacier front is advancing or not. This is balanced by the extent of the reservoir areas which are larger than those of the receiving area.

At a larger scale, we compare the individual glacier average elevation change between Hugonnet et al. (2021) and this workflow for the period 2005-2015 (Figure C2). The mean elevation changes are more negative with our workflow (by about 0.44 m for the median value). The discrepancy is larger for surge-type glaciers than for non-surge-type ones (0.57 and 0.31 m with standard deviations of 1.1 and 1.02 m, respectively). Considering the better retrieval of positive elevation changes of our workflow for surges, we would expect a positive discrepancy for surge-type glaciers. A number of glaciers have artefacts in our dataset, especially negative elevation changes in accumulation areas. At regional scale and possibly glacier scale, the noise impact may exceeds the impact of the better retrieval of positive changes of the few surge events happening during this period. For calculating geodetic glacier mass balance, the Hugonnet et al. (2021) dataset is therefore the preferred choice for non-surge-type glaciers or quiescent periods, and a validation of the elevation interpolated by our method is recommended.

5.4 Methodological Insights and Modifications

In the development of the workflow, we first tried adapting Gaussian Process Regression (GP regression) like the original study instead of ALPS. Our limitation with GP regression lies in the kernel definition which is done according to the variance of elevation changes. Each surge event is different in variances, which is also very different from the data variance in quiescent periods or on non-surge-type glaciers. We tried different settings of the kernels, that differs from the study of Hugonnet et al. (2021). We removed the seasonal component of the model (exponential sine-squared (ESS) kernel). The length scale and the magnitude parameters of the remaining components were manually tuned after testing. We added radial basis function (RBF) components of length scales of few months and with a variance of a few tens/hundreds of square meters. The kernels that provided a suitable interpolation were slightly outperformed by the ALPS-REML algorithm. This could be reevaluated for other datasets (for e.g. less noisy), more complex GP regression processes or future advances.

https://doi.org/10.5194/egusphere-2024-3480
Preprint. Discussion started: 6 December 2024

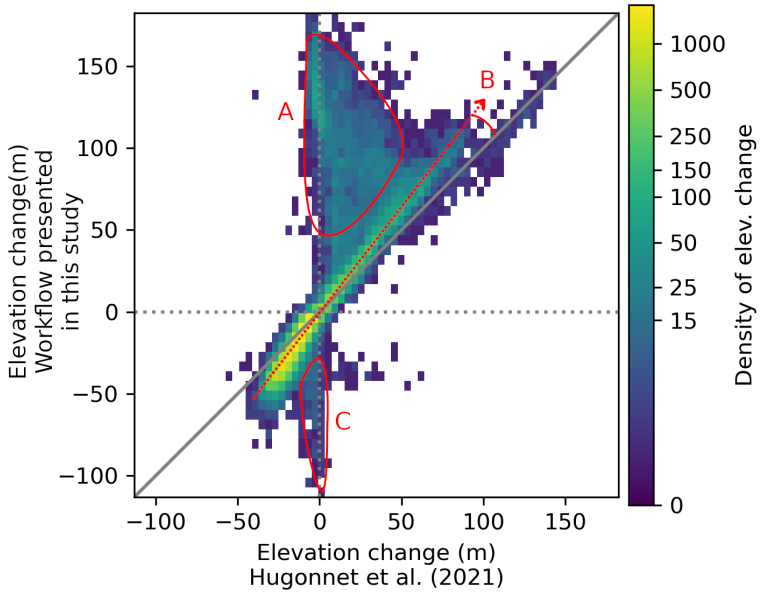

Figure 12. Histogram of interpolated elevation change comparison over 8 surges between the original processing from Hugonnet et al. (2021) and this workflow. The superimposed histograms of the 8 surge events are represented individually in appendix Fig. C1. The elevation changes are retrieved over the surge-affected areas and the surge period estimated from the Hovmöller diagrams of this workflow.

Finally, we discuss here the feasibility to modify the proposed workflow to be used on different datasets, possibly including several data sources to increase temporal resolution (i.e. from DEMs from different sensors). Even in the case of a similar ASTER DEM dataset processed differently, with lower noise/higher precision, several changes may be done to adapt the filtering. A diminution of the span parameter along with a a diminution of the filter threshold in the LOWESS workflow should be tested. Abandoning morphological erosion should also be considered, as it answers to the behaviour of our specific photogrammetric processing. It may not be beneficial for DEMs where outliers does less alter neighbouring pixels, regarding the number of pixels it removes. The use of weighting could also be abandoned in the case of more precise DEMs, as the uncertainty values are not completely representative of the confidence in the measurement. The ALPS-REML prediction parameters could remain as it is, although other values of the hyperparameters degree of the basis functions p and the order of penalty q can be modified to adjust the smoothing and border effects. More complex considerations would be required in the case of several data sources. More particularly, the weighting may be defined differently to ensure a consistency between the dataset.

6 Conclusions

We present a new workflow to process DEM time series of high temporal resolution that is specifically designed to preserve the elevation signal of glacier surge events. We applied the workflow to a dataset from the ASTER sensor over 2000-2019. We filter the data with a LOWESS algorithm, which preserves the surge signal. Some filter issues can appear in difficult areas, which

https://doi.org/10.5194/egusphere-2024-3480
Preprint. Discussion started: 6 December 2024

are often not located in surge-affected areas (e.g. textureless accumulation areas, steep slopes). The elevation interpolation (B-spline method ALPS-REML) allows for the observation of surge dynamics, and the estimate of mass transfers at a few months interval. Some surge events covered by only a small number of DEMs can be smoothed, resulting in an underestimation of the surface elevation change and surge duration. Over our study area in the Karakoram range (HMA), our method provides interpolated time series for 80% of the pixels belonging to glacier area. Our workflow is able to preserve surge events in a better way than the original non-specific workflow. The resulting data compares fairly well with independent studies on several events, except in a few cases. We have discrepancies in estimated volume transferred compared to previous studies ranging from 2% to 19% on two surge events and four volumes transferred, 64% on the Khurdopin surge. It creates a unique dataset able to represent thickness changes of surge events at a months scale over a regional extent. It opens new possibilities for combined analysis of surges with elevation and velocity datasets, or to follow the evolution of surface slope and more complex variables.

Code and data availability. Although not explained in the original paper Shekhar et al. (2021), the authors of ALPS do provide the code for fitting ALPS both with GCV and REML in the repository Shekhar (2020). The code of this workflow can be found on the repository https://doi.org/10.5281/zenodo.14045605 (Beraud et al., 2024). Some sample of elevation change maps and surge-affected areas of the four selected glaciers are also available on the repository.

Appendix A: Additional time series

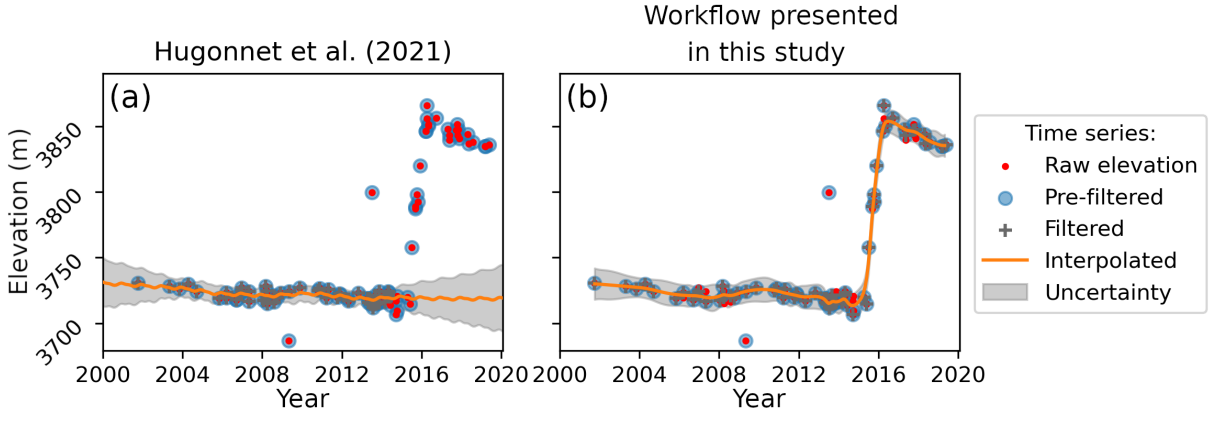

Figure A1. a-b: additional time series complementing the figure Fig. 6, at coordinates (36.126, 75.158) over the Hispar glacier.

https://doi.org/10.5194/egusphere-2024-3480
Preprint. Discussion started: 6 December 2024

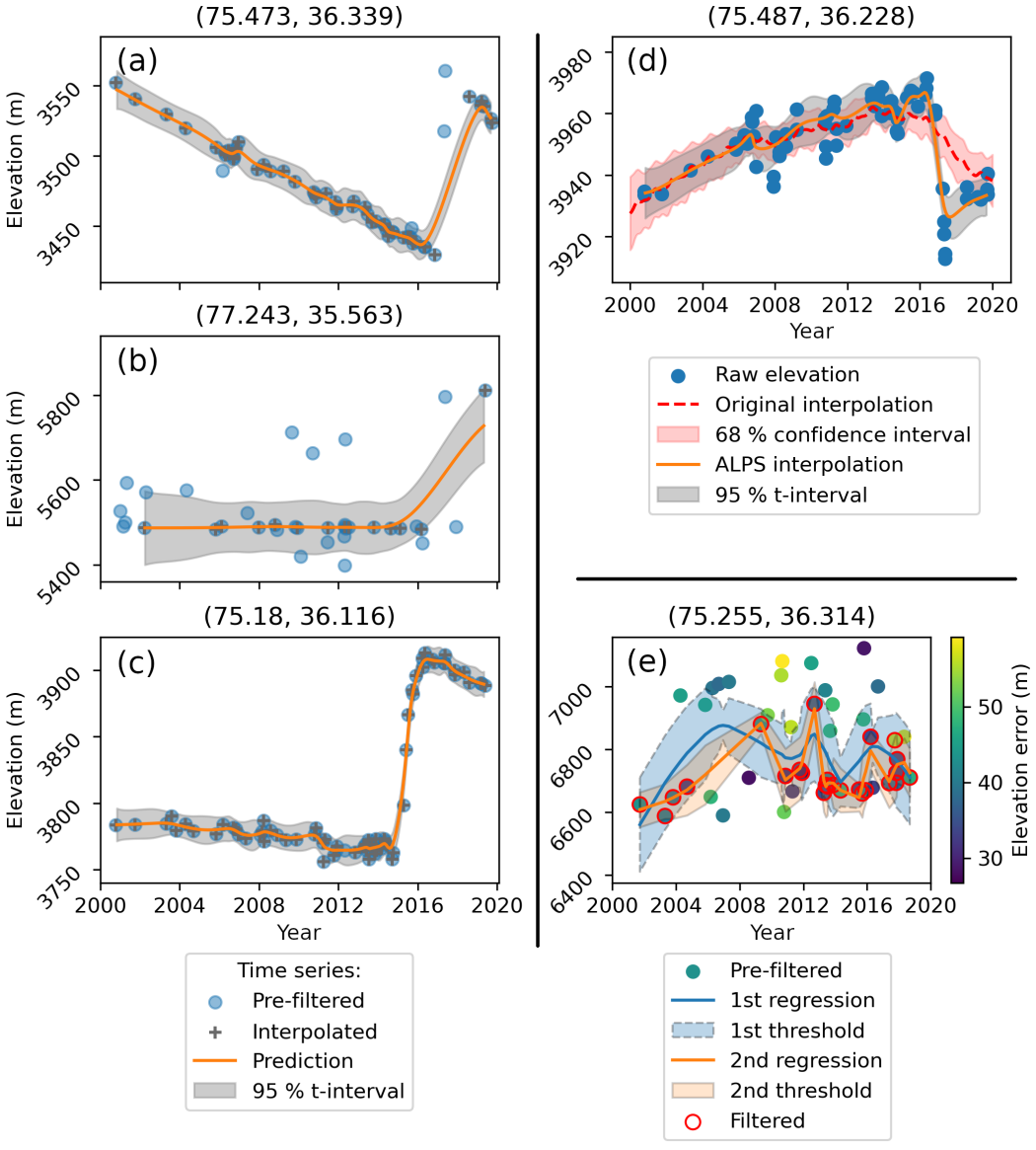

Figure A2. Additional time series. Panels a-c show more examples of ALPS-REML interpolation with distinct flaws. The panel d compares the interpolation results of Hugonnet et al. (2021) ("Original interpolation" and its confidence interval) and this study ("ALPS interpolation" and its t-interval). The panel e show the successive iteration of the LOWESS regression, with points coloured by their estimated error (weight of the regression).

https://doi.org/10.5194/egusphere-2024-3480
Preprint. Discussion started: 6 December 2024

Appendix B: Volume transferred on original ASTER data

Glacier RGI 7.0 code	Date start	Date end	Reservoir vol. change	Receiving vol. change	Imbalance	Data gap [after interp.]
Hispar 21670	2014-01	2016-09	-1593 x 10^6 m^3	1123 x 10^6 m^3	-470 x 10^6 m^3 -3.05 m	1.1% [0%]
Yazghil 21865	2003-07	2007-01	-38 x 10^6 m^3	34 x 10^6 m^3	-4 x 10^6 m^3 -0.29 m	0.1% [0%]
Khurdopin 14958	2016-03	2019-03	-587 x 10^6 m^3	451 x 10^6 m^3	-135 x 10^6 m^3 -2.86 m	0% [0%]
Kyagar 14958	2012-11	2017-01	-191 x 10^6 m^3	199 x 10^6 m^3	8 x 10^6 m^3 0.27 m	0% [0%]

Table B1. Volume transferred of surges for the four selected glaciers this time according to the original interpolated ASTER dataset from Hugonnet et al. (2021), during the same period as in the table 1.

https://doi.org/10.5194/egusphere-2024-3480
Preprint. Discussion started: 6 December 2024

Appendix C: Volume transferred and mass balance comparison

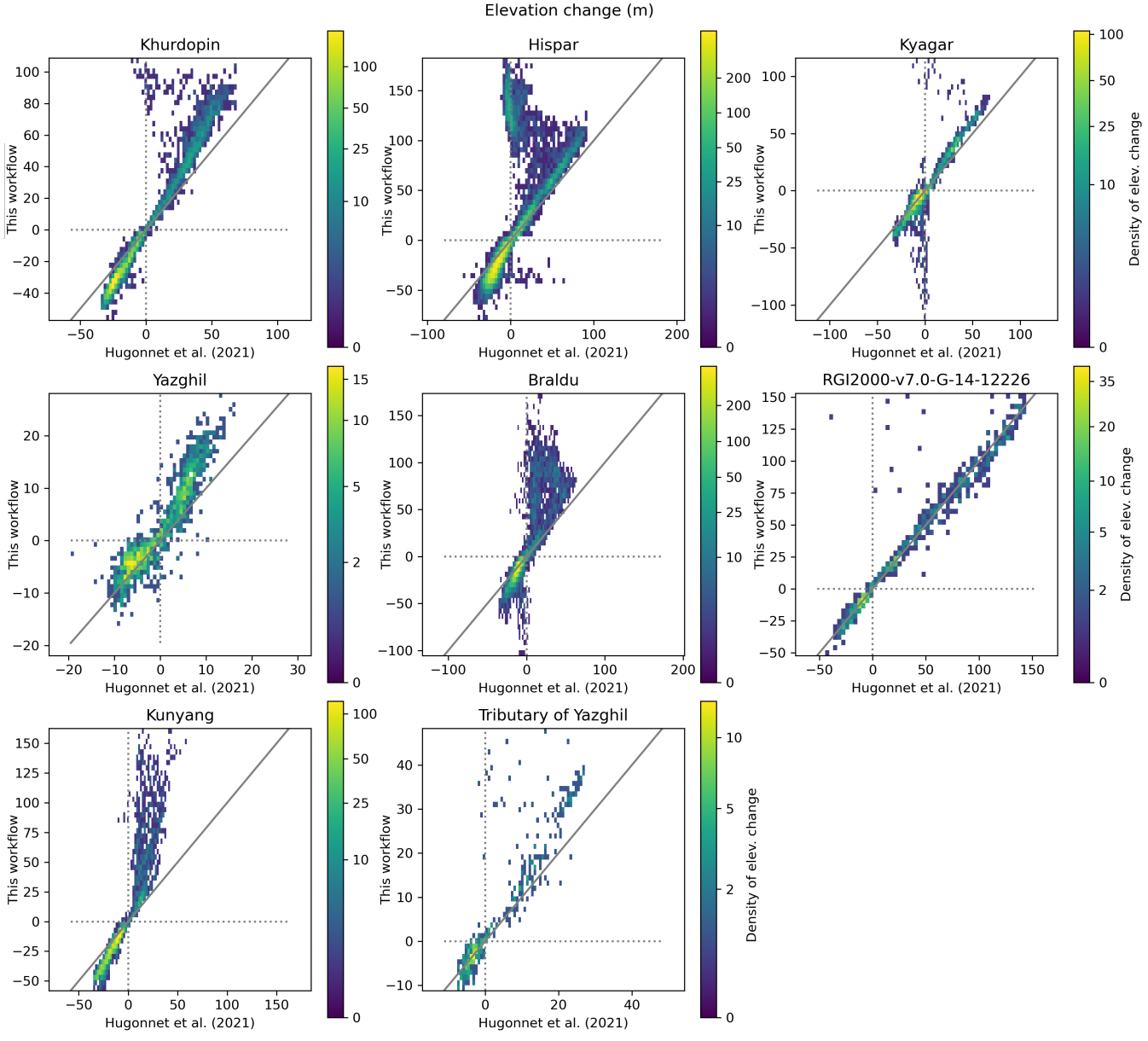

Figure C1. Individual representation of Fig. 12, elevation change comparison histogram per surge. Each surge is the single one occurring during our study period on the glacier designated, except for Yazghil glacier for which the surge is the 2003-2007 one. Note that the reservoir area of the unnamed glacier (RGI code RGI2000-v7.0-G-14-12226) is captured over only a third of its extent here.

https://doi.org/10.5194/egusphere-2024-3480
Preprint. Discussion started: 6 December 2024

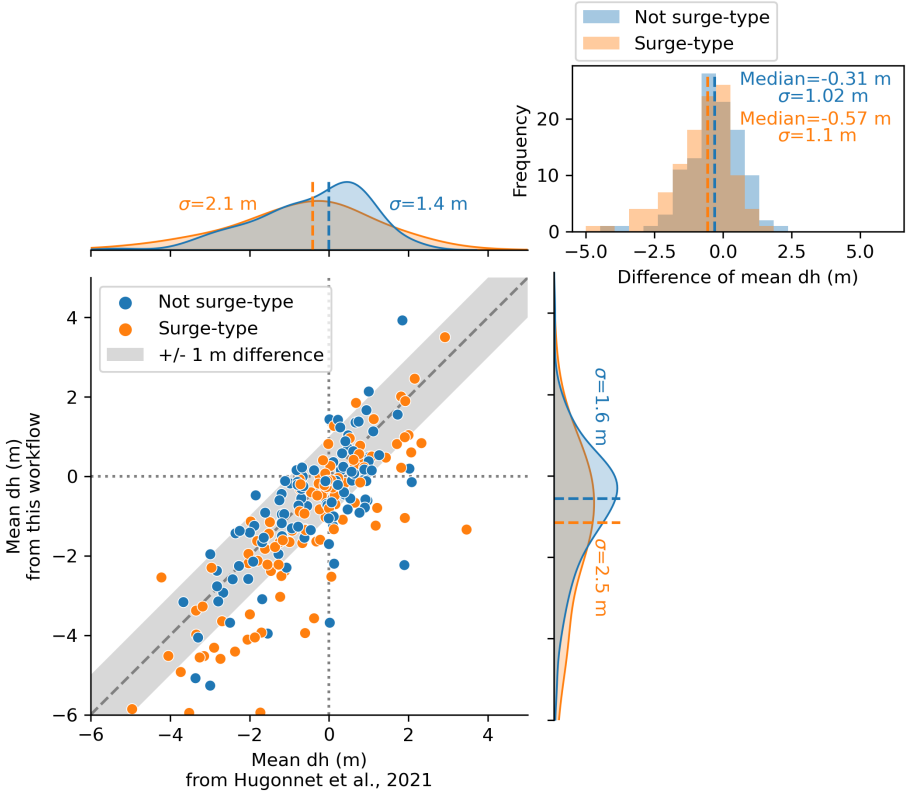

Figure C2. Comparison of mean elevation change (dh in the figure) per glacier from 2005 to 2015, between the interpolated dataset of Hugonnet et al. (2021) and this workflow. It is calculated over the same valid pixels to avoid different data gaps. It represents 224 glaciers in the center of Karakoram, with 112 glaciers in each surge and non-surge type category. We extract surge-type glaciers from the inventories of Guillet et al. (2022) and Guo et al. (2022) (categories I and II during 2000-2020). The top right histogram represents the difference of mean dh between the two datasets. The dotted lines represent the median of the distributions. The sigma symbol represents the standard deviation.

Author contributions. Luc Beraud: Conceptualization, Methodology, Software, Writing - Original Draft. Fanny Brun and Amaury Dehecq: Conceptualization, Methodology, Writing - Review & Editing, Supervision. Romain Hugonnet and Prashant Shekhar: Software, Writing - Review & Editing.

Competing interests. The authors declare no competing interest.

Acknowledgements. We are grateful to Laurane Charrier for her suggestions and methodological discussions. We thank Etienne Berthier (CNRS, LEGOS) for providing SPOT DEMs and discussing the methodology of the work. We thank also Jakob Steiner for our discussion

https://doi.org/10.5194/egusphere-2024-3480
Preprint. Discussion started: 6 December 2024

and his input related to his published work. We finally thank the French program Programme National de Télédétection Spatiale (PNTS) for its funding support.

https://doi.org/10.5194/egusphere-2024-3480
Preprint. Discussion started: 6 December 2024

References

Beaud, F., Aati, S., Delaney, I., Adhikari, S., and Avouac, J.-P.: Surge dynamics of Shisper Glacier revealed by time-series correlation of optical satellite images and their utility to substantiate a generalized sliding law, The Cryosphere, 16, 3123–3148, https://doi.org/10.5194/tc-16-3123-2022, 2022.

Benn, D. I., Hewitt, I. J., and Luckman, A. J.: Enthalpy balance theory unifies diverse glacier surge behaviour, Annals of Glaciology, pp. 1–7, https://doi.org/10.1017/aog.2023.23, 2023.

Beraud, L., Brun, F., Dehecq, A., Hugonnet, R., and Shekhar, P.: Data and code for the publication of a surge-specific DEM workflow on ASTER DEMs., https://doi.org/10.5281/ZENODO.14045605, 2024.

Berthier, E. and Brun, F.: Karakoram geodetic glacier mass balances between 2008 and 2016: persistence of the anomaly and influence of a large rock avalanche on Siachen Glacier, Journal of Glaciology, 65, 494–507, https://doi.org/10.1017/jog.2019.32, 2019.

Bhambri, R., Hewitt, K., Kawishwar, P., and Pratap, B.: Surge-type and surge-modified glaciers in the Karakoram, Scientific Reports, 7, 15 391, https://doi.org/10.1038/s41598-017-15473-8, 2017.

Bhambri, R., Hewitt, K., Haritashya, U. K., Chand, P., Kumar, A., Verma, A., Tiwari, S. K., and Rai, S. K.: Characteristics of surge-type tributary glaciers, Karakoram, Geomorphology, 403, 108 161, https://doi.org/10.1016/j.geomorph.2022.108161, 2022.

Brun, F., Berthier, E., Wagnon, P., Kääb, A., and Treichler, D.: A spatially resolved estimate of High Mountain Asia glacier mass balances from 2000 to 2016, Nature Geoscience, 10, 668–673, https://doi.org/10.1038/ngeo2999, 2017.

Charrier, L., Yan, Y., Koeniguer, E. C., Leinss, S., and Trouve, E.: Extraction of Velocity Time Series With an Optimal Temporal Sampling From Displacement Observation Networks, IEEE Transactions on Geoscience and Remote Sensing, 60, 1–10, https://doi.org/10.1109/TGRS.2021.3128289, 2022.

Cleveland, W. S. and Devlin, S. J.: Locally Weighted Regression: An Approach to Regression Analysis by Local Fitting, Journal of the American Statistical Association, 83, 596–610, https://doi.org/10.1080/01621459.1988.10478639, 1988.

Crompton, J. W., Flowers, G. E., and Stead, D.: Bedrock Fracture Characteristics as a Possible Control on the Distribution of Surge-Type Glaciers, Journal of Geophysical Research: Earth Surface, 123, 853–873, https://doi.org/10.1002/2017JF004505, 2018.

Cuffey, K. M. and Paterson, W. S. B.: The Physics of Glaciers, Elsevier Science, Burlington, 4th ed edn., ISBN guill, oCLC: 761646843, 2010.

Derkacheva, A., Mouginot, J., Millan, R., Maier, N., and Gillet-Chaulet, F.: Data Reduction Using Statistical and Regression Approaches for Ice Velocity Derived by Landsat-8, Sentinel-1 and Sentinel-2, Remote Sensing, 12, 1935, https://doi.org/10.3390/rs12121935, 2020.

Echelmeyer, K., Butterfield, R., and Cuillard, D.: Some Observations on a Recent Surge of Peters Glacier, Alaska, U.S.A., Journal of Glaciology, 33, 341–345, https://doi.org/10.3189/S0022143000008935, 1987.

European Space Agency and Airbus: Copernicus DEM, https://doi.org/10.5270/ESA-c5d3d65, institution: European Space Agency, 2022.

Gao, Y., Wang, J., Liu, S., Yao, X., Qi, M., Liang, P., Xie, F., Mu, J., and Ma, X.: Monitoring dynamics of Kyagar Glacier surge and repeated draining of Ice-dammed lake using multi-source remote sensing, Science of The Total Environment, 928, 172 467, https://doi.org/10.1016/j.scitotenv.2024.172467, 2024.

Gardner, A., Fahnestock, M., and Scambos, T.: MEaSUREs ITS_LIVE Landsat Image-Pair Glacier and Ice Sheet Surface Velocities, Version 1, https://doi.org/10.5067/IMR9D3PEI28U, 2022.

Girod, L., Nuth, C., Kääb, A., McNabb, R., and Galland, O.: MMASTER: Improved ASTER DEMs for Elevation Change Monitoring, Remote Sensing, 9, 704, https://doi.org/10.3390/rs9070704, 2017.

https://doi.org/10.5194/egusphere-2024-3480
Preprint. Discussion started: 6 December 2024

Guillet, G., King, O., Lv, M., Ghuffar, S., Benn, D., Quincey, D., and Bolch, T.: A regionally resolved inventory of High Mountain Asia surge-type glaciers, derived from a multi-factor remote sensing approach, The Cryosphere, 16, 603–623, https://doi.org/10.5194/tc-16-603-2022, 2022.

Guo, L., Li, J., Li, Z., Wu, L., Li, X., Hu, J., Li, H., Li, H., Miao, Z., and Li, Z.: The Surge of the Hispar Glacier, Central Karakoram: SAR 3-D Flow Velocity Time Series and Thickness Changes, Journal of Geophysical Research: Solid Earth, 125, https://doi.org/10.1029/2019JB018945, 2020.

Guo, L., Li, J., Dehecq, A., Li, Z., Li, X., and Zhu, J.: A new inventory of High Mountain Asia surge-type glaciers derived from multiple elevation datasets since the 1970s, preprint, ESSD – Ice/Glaciology, https://doi.org/10.5194/essd-2022-238, 2022.

Herreid, S. and Truffer, M.: Automated detection of unstable glacier flow and a spectrum of speedup behavior in the Alaska Range, Journal of Geophysical Research: Earth Surface, 121, 64–81, https://doi.org/10.1002/2015JF003502, 2016.

Hugonnet, R., McNabb, R., Berthier, E., Menounos, B., Nuth, C., Girod, L., Farinotti, D., Huss, M., Dussaillant, I., Brun, F., and Kääb, A.: Accelerated global glacier mass loss in the early twenty-first century, Nature, 592, 726–731, https://doi.org/10.1038/s41586-021-03436-z, 2021.

Hugonnet, R., Brun, F., Berthier, E., Dehecq, A., Mannerfelt, E. S., Eckert, N., and Farinotti, D.: Uncertainty Analysis of Digital Elevation Models by Spatial Inference From Stable Terrain, IEEE Journal of Selected Topics in Applied Earth Observations and Remote Sensing, 15, 6456–6472, https://doi.org/10.1109/JSTARS.2022.3188922, 2022.

Imran, M. and Ahmad, U.: Geospatially analysing the dynamics of the Khurdopin Glacier surge using multispectral and temporal remote sensing and ground observations, Natural Hazards, 108, 847–866, https://doi.org/10.1007/s11069-021-04708-7, 2021.

Kotlyakov, V. M., Chernova, L. P., Khromova, T. E., Muraviev, A. Y., Kachalin, A. B., and Tiuflin, A. S.: Unique Surges of Medvezhy Glacier, Doklady Earth Sciences, 483, 1547–1552, https://doi.org/10.1134/S1028334X18120152, 2018.

Lai, Y.-R. and Wang, L.: Monthly Surface Elevation Changes of the Greenland Ice Sheet From ICESat-1, CryoSat-2, and ICESat-2 Altimetry Missions, IEEE Geoscience and Remote Sensing Letters, 19, 1–5, https://doi.org/10.1109/LGRS.2021.3058956, 2022.

Li, G., Lv, M., Quincey, D. J., Taylor, L. S., Li, X., Yan, S., Sun, Y., and Guo, H.: Characterizing the surge behaviour and associated ice-dammed lake evolution of the Kyagar Glacier in the Karakoram, Tech. rep., Glaciers/Remote Sensing, https://doi.org/10.5194/tc-2022-253, 2023.

Lovell, A. M., Carr, J. R., and Stokes, C. R.: Topographic controls on the surging behaviour of Sabche Glacier, Nepal (1967 to 2017), Remote Sensing of Environment, 210, 434–443, https://doi.org/10.1016/j.rse.2018.03.036, 2018.

Nolan, A., Kochtitzky, W., Enderlin, E. M., McNabb, R., and Kreutz, K. J.: Kinematics of the exceptionally-short surge cycles of Sít' Kusá (Turner Glacier), Alaska, from 1983 to 2013, Journal of Glaciology, 67, 744–758, https://doi.org/10.1017/jog.2021.29, 2021.

Paul, F.: Revealing glacier flow and surge dynamics from animated satellite image sequences: examples from the Karakoram, The Cryosphere, 9, 2201–2214, https://doi.org/10.5194/tc-9-2201-2015, 2015.

Paul, F., Strozzi, T., Schellenberger, T., and Kääb, A.: The 2015 Surge of Hispar Glacier in the Karakoram, Remote Sensing, 9, 888, https://doi.org/10.3390/rs9090888, 2017.

Paul, F., Piermattei, L., Treichler, D., Gilbert, L., Girod, L., Kääb, A., Libert, L., Nagler, T., Strozzi, T., and Wuite, J.: Three different glacier surges at a spot: what satellites observe and what not, The Cryosphere, 16, 2505–2526, https://doi.org/10.5194/tc-16-2505-2022, 2022.

Rizzoli, P., Martone, M., Gonzalez, C., Wecklich, C., Borla Tridon, D., Bräutigam, B., Bachmann, M., Schulze, D., Fritz, T., Huber, M., Wessel, B., Krieger, G., Zink, M., and Moreira, A.: Generation and performance assessment of the global TanDEM-X digital elevation model, ISPRS Journal of Photogrammetry and Remote Sensing, 132, 119–139, https://doi.org/10.1016/j.isprsjprs.2017.08.008, 2017.

https://doi.org/10.5194/egusphere-2024-3480
Preprint. Discussion started: 6 December 2024

Round, V., Leinss, S., Huss, M., Haemmig, C., and Hajnsek, I.: Surge dynamics and lake outbursts of Kyagar Glacier, Karakoram, The Cryosphere, 11, 723–739, https://doi.org/10.5194/tc-11-723-2017, 2017.

Rupnik, E., Daakir, M., and Pierrot Deseilligny, M.: MicMac – a free, open-source solution for photogrammetry, Open Geospatial Data, Software and Standards, 2, 14, https://doi.org/10.1186/s40965-017-0027-2, 2017.

Ruppert, D., Wand, M. P., and Carroll, R. J.: Semiparametric regression, Cambridge series in statistical and probabilistic mathematics, Cambridge Univ. Press, Cambridge, repr edn., ISBN 978-0-521-78050-6 978-0-521-78516-7, 2009.

Sevestre, H. and Benn, D. I.: Climatic and geometric controls on the global distribution of surge-type glaciers: implications for a unifying model of surging, Journal of Glaciology, 61, 646–662, https://doi.org/10.3189/2015JoG14J136, 2015.

Shean, D.: High Mountain Asia 8-meter DEM Mosaics Derived from Optical Imagery, Version 1, https://doi.org/10.5067/KXOVQ9L172S2, 2017.

Shean, D. E., Bhushan, S., Montesano, P., Rounce, D. R., Arendt, A., and Osmanoglu, B.: A Systematic, Regional Assessment of High Mountain Asia Glacier Mass Balance, Frontiers in Earth Science, 7, 363, https://doi.org/10.3389/feart.2019.00363, 2020.

Shekhar, P.: ALPS code, https://github.com/p-shekhar/ALPS, gitHub repository, 2020.

Shekhar, P., Csatho, B., Schenk, T., Roberts, C., and Patra, A. K.: ALPS: A Unified Framework for Modeling Time Series of Land Ice Changes, IEEE Transactions on Geoscience and Remote Sensing, 59, 6466–6481, https://doi.org/10.1109/TGRS.2020.3027190, 2021.

Steiner, J. F., Kraaijenbrink, P. D. A., Jiduc, S. G., and Immerzeel, W. W.: Brief communication: The Khurdopin glacier surge revisited – extreme flow velocities and formation of a dammed lake in 2017, The Cryosphere, 12, 95–101, https://doi.org/10.5194/tc-12-95-2018, 2018.

Terleth, Y., Van Pelt, W. J. J., Pohjola, V. A., and Pettersson, R.: Complementary Approaches Towards a Universal Model of Glacier Surges, Frontiers in Earth Science, 9, 732 962, https://doi.org/10.3389/feart.2021.732962, 2021.

Thøgersen, K., Gilbert, A., Bouchayer, C., and Schuler, T. V.: Glacier Surges Controlled by the Close Interplay Between Subglacial Friction and Drainage, Journal of Geophysical Research: Earth Surface, 129, e2023JF007 441, https://doi.org/10.1029/2023JF007441, 2024.

Turrin, J., Forster, R. R., Larsen, C., and Sauber, J.: The propagation of a surge front on Bering Glacier, Alaska, 2001–2011, Annals of Glaciology, 54, 221–228, https://doi.org/10.3189/2013AoG63A341, 2013.

Wahba, G.: Spline Models for Observational Data, Society for Industrial and Applied Mathematics, ISBN 978-0-89871-244-5 978-1-61197-012-8, https://doi.org/10.1137/1.9781611970128, 1990.

Wang, D. and Kääb, A.: Modeling Glacier Elevation Change from DEM Time Series, Remote Sensing, 7, 10 117–10 142, https://doi.org/10.3390/rs70810117, 2015.

Wang, Q., Yi, S., and Sun, W.: Continuous Estimates of Glacier Mass Balance in High Mountain Asia Based on ICESat-1,2 and GRACE/-GRACE Follow-On Data, Geophysical Research Letters, 48, e2020GL090 954, https://doi.org/10.1029/2020GL090954, 2021.

Wendt, A., Mayer, C., Lambrecht, A., and Floricioiu, D.: A Glacier Surge of Bivachny Glacier, Pamir Mountains, Observed by a Time Series of High-Resolution Digital Elevation Models and Glacier Velocities, Remote Sensing, 9, 388, https://doi.org/10.3390/rs9040388, 2017.

Yue, L., Chao, N., Chen, G., Chen, L., Zhang, B., Sun, R., Zhang, Y., Wang, S., Wang, Z., Li, F., Yu, N., and Ouyang, G.: Reconstructing Continuous Ice Sheet Elevation Changes in the Amundsen Sea Sector During 2003–2021 by Merging Envisat, ICESat, CryoSat-2, and ICESat-2 Multi-Altimeter Observations, Journal of Geophysical Research: Earth Surface, 128, e2022JF007 020, https://doi.org/10.1029/2022JF007020, 2023.

Zhang, Z., Zhao, J., Liu, S., Zhang, Q., Jiang, Z., Xu, Y., and Su, H.: Characterization of Three Surges of the Kyagar Glacier, Karakoram, Remote Sensing, 15, 2113, https://doi.org/10.3390/rs15082113, 2023.